

POLITECNICO DI TORINO

Department of Mechanical and Aerospace Engineering
Master of Science degree in Mechanical Engineering

Master of Science Thesis

**Radial turbine geometrical parameters optimization based on
CFD analysis and application to engine performance assessment**



Mentors

Prof. Mirko Baratta
Prof. Dmytro Samoilenko

Candidate

Andrea Occhipinti

April 2019

*Dedicated to my family,
for all their support and inspiration*

Statement

As author of the thesis entitled:

Radial turbine geometrical parameters optimization based on CFD analysis and application to engine performance assessment

which I have done myself, observing the rules of intellectual property protection, I allow my work to be made public and I agree to make it available in the Library of the Faculty of Automotive and Construction Machinery Engineering of the Warsaw University of Technology as part of the statutory tasks of the library.

Contents

Abstract	13
1 Introduction	14
1.1 Background	14
1.2 Turbocharger fundamentals	15
1.2.1 Working principle	15
1.2.2 Compressor side	16
1.2.3 Turbine side	17
1.3 Turbocharging techniques	19
1.4 CFD analysis software	21
1.4.1 SOLIDWORKS FloXpress™	22
1.4.2 SOLIDWORKS Flow Simulation™	22
1.4.3 GT-POWER Suite™	22
2 Literature review	23
2.1 Radial turbine theory	23
2.1.1 Governing equations	23
2.1.2 Fluid specific work	27
2.1.3 Volute	27
2.2 Solidworks - Computational architecture	28
2.2.1 Governing equations	28
2.2.2 Laminar/turbulent boundary model	29
2.2.3 Mesh	29
2.3 GT-Power model implementation	31
2.3.1 Maps evaluation	32
3 Model description	34

3.1	Geometry overview	34
3.1.1	Wheel's trim	35
3.1.2	Turbine housing A/R	36
3.2	Reference data	38
4	SolidWorks simulation setup	39
4.1	Computational domain creation	39
4.1.1	Fluid check	40
4.2	FloXpress pre-analysis	40
4.2.1	Result	41
4.3	Flow Simulation	42
4.3.1	Analysis type	42
4.3.2	Fluid	43
4.3.3	Wall and initial conditions	44
4.3.4	Computational domain and mesh	44
4.3.5	Boundary conditions	45
4.3.6	Goals & convergence	46
5	SolidWorks - Calculations	47
5.1	Methodology	47
5.2	Results	48
5.2.1	Fluid - Air	49
5.2.2	Fluid - Exhaust gas	51
5.3	Plots	53
6	GT-Power engine model	56
6.1	Internal combustion engine	57
6.2	Turbocharger	58
6.3	Standard turbine simulation	59
7	Turbine size impact on BSFC	61
7.1	Mass multiplier scaling method	61
7.2	Fluid-dynamic similitude scaling method	64
7.2.1	Consideration about methods usage	66

7.3	Further turbine simulations	66
7.3.1	Turbine size x0.9	66
7.3.2	Turbine size x1.1	68
7.4	Results comparison	69
7.5	Medium load deterioration analysis	71
7.5.1	Turbine expansion ratio β	72
7.5.2	Pumping loop	73
7.6	Control strategy	74
7.7	Maximum braking torque	78
8	Conclusions	82
8.1	Future work	83
8.2	Contribution	84
	Bibliography	85

List of Figures

1.1	Turbocharger - Engine system schematic [2]	15
1.2	Turbocharger schematic	16
1.3	Compressor performance map [3]	17
1.4	Turbine efficiency map [5]	18
1.5	Turbine performance map [5]	18
1.6	BorgWarner's eBooster scheme [3]	21
2.1	h-s diagram of the process of a radial turbine [7]	25
2.2	Turbine performance map [6]	26
2.3	Computational mesh near the solid/fluid interface [8]	30
2.4	Orthogonality for quadrilateral and triangular faced elements	31
2.5	Turbine maps fitting curves, 1 [13]	32
2.6	Turbine maps fitting curves, 2 [13]	32
3.1	Turbocharger model	34
3.2	Turbocharger front section	35
3.3	Inducer / Exducer for turbine and compressor's wheel	35
3.4	A/R compressor illustration [10]	36
3.5	A/R turbine housing illustration	37
3.6	Exhaust gas flow chart - Garrett GT3071R [10]	38
4.1	Lids' creation to isolate volute domain	39
4.2	Fluid domain	40
4.3	FloXpress fluid simulation result	41
4.4	SolidWorks Flow Simulation analysis setup	42
4.5	Engineering Database exhaust gas implementation [11]	43
4.6	Mesh and Computational Domain visualization	45
4.7	Boundary conditions setup	46

5.1	Exhaust gas flow chart - Working point	47
5.2	Boundary conditions setup	49
5.3	Pressure results using Air as simulation fluid	50
5.4	Velocity results using Air as simulation fluid	50
5.5	Pressure results using Exhaust gas as simulation fluid	51
5.6	Velocity results using Exhaust gas as simulation fluid	52
5.7	Temperature drop using a non-adiabatic system	52
5.8	Pressure contour plot	53
5.9	Density contour plot	54
5.10	Pressure flow trajectories	54
5.11	Velocity flow trajectories	55
6.1	Model case setup	56
6.2	GT-Power engine model	57
6.3	GT-Power turbocharger model	58
6.4	Standard turbine BSFC trend	60
7.1	Map creation window - GT-Power	62
7.2	BSFC trend comparison, $mm = 0.824$	63
7.3	Fluid-dynamic scaled turbine map - 1	65
7.4	Fluid-dynamic scaled turbine map - 2	65
7.5	BSFC trend comparison, $mm = 0.908$	67
7.6	BSFC trend comparison, $mm = 1.100$	69
7.7	Efficiency runouts compared to basic turbine	70
7.8	BSFC trends comparison	71
7.9	Different turbine expansion ratios comparison	72
7.10	Exhaust pressure at different regimes	73
7.11	Pressure and MFB trends	74
7.12	PID controller scheme	75
7.13	PID setting window	75
7.14	MFB50 trend comparison	76
7.15	SOI angle using MFB50 control strategy	76
7.16	Injected mass using MFB50 control strategy	77
7.17	BSFC trend using MFB50 control strategy	77

7.18 Load PID controller setting window	78
7.19 Maximum Power and Torque compared to standard engine	79
7.20 BMEP trend for maximum performance and standard engine	80
7.21 Cylinder pressure trend for maximum performance and standard engine	80
7.22 Air-to-Fuel ratio	81

Nomenclature

Abbreviations

BC Boundary Condition

CAD Computer Aided Design

CFD Computational Fluid Dynamics

CHRA Center Housing and Rotating Assembly

NEDC New European Driving Cycle

RANS Reynolds Averaged Navier Stokes

URANS Unsteady Reynolds Averaged Navier Stokes

VGT Variable Geometry Turbo

WLTP Worldwide harmonized Light vehicles Test Procedure

Greek Symbols

β Expansion ratio

δ_{ij} Identity matrix

η_C Compressor efficiency

η_T Turbine efficiency

μ Dynamic viscosity

Ω Angular velocity

ρ Density

τ_A Axial torque

θ Diffuser angle

Roman Symbols

\dot{m} Mass flow rate

\dot{Q} Thermal power

\dot{W}_t Shaft work

A Cross sectional area

c Fluid velocity

c_p Gas specific heat, constant pressure

E Energy

g Gravitational constant

h Enthalpy

I Rothalpy

k Specific heat ratio

M Mach number

m Mass

n Normal vector

p Pressure

Q Heat transfer

r Radius

R_g Gas constant

T Temperature

U Blade velocity, Mean velocity

u Velocity

W Work

w Relative velocity

z Height

Subscripts

θ Tangential direction

i, j, k Direction

rel Relative property

0 Stagnation property, Volute inlet

1 Stator inlet

2 Stator throat

3 Stator outlet

4 Rotor inlet

5 Rotor throat

6 Rotor outlet

7 Diffuser outlet

Abstract

The current trend of vehicle manufacturers is increasingly driven towards the use of downsizing technology, which coupled with turbocharging technique, allows to obtain engines with higher power densities and characteristics in terms of emissions, performance and fuel consumption much better than a conventional engine. The achievement of this target is clearly not any easy task for developers which have to perform a considerable amount of studies to optimize the system and find the compromise which best fits all requirements. Therefore, fluid dynamic analysis, using dedicated CFD softwares, in addition to experimental tests, are fundamental for the analysis and optimization of engine turbomatching: the former in particular becomes essential considering the lack of data often available and the huge amount of time required at the test bench.

The objective of the thesis was to develop a methodology that could be used for radial turbine geometrical parameters optimization based on CFD analysis and its application to engine performance assessment. Initially, 3D fluid dynamic studies will be performed on the model, in order to evaluate the actual behaviour of the component, in terms of pressure and temperature drop and gather useful data. Afterwards, collected information will be used to simulate the response of the system using the overall model of the engine created through GT-Power in a 0-dimensional approach, firstly evaluating the standard turbine and then rating the impact that geometry changes on turbine design could have on overall engine performance.

Keywords: Turbocharger, turbomatching, turbine, CFD, GT-Power, SolidWorks, SolidWorks Flow Simulation, geometrical turbine parameters, turbine characteristics

Chapter 1

Introduction

1.1 Background

Nowadays more and more importance is placed on improving performance and emissions of engines due to the global move to reduce CO_2 emissions, where the target for 2021 is set to < 95 [g/km], with further reduction of 15% and 37.5% expected respectively by 2025 and 2030. Car manufacturers has to strictly follow regulations to homologate new vehicles in terms of pollutant emissions, following specific driving cycles, such as NEDC (New European Driving Cycle) or WLTP (Worldwide Harmonized Light-Duty Vehicle Test Procedure) which has become the new European standard.

Turbocharging technique is crucial to achieve and improve these aspects, mainly by enabling engine's downsizing (usage of a smaller engine capable to deliver the same power of a bigger one). Moreover, one of the biggest source of inefficiency of the combustion process is the significant amount of fuel energy wasted through the exhaust. Turbochargers recover some of that energy to increase intake pressure, improving power density and efficiency. Therefore, it is necessary to develop an optimum turbocharging system, to suit the engine requirements.

"Computational fluid dynamics or CFD is the analysis of systems involving fluid flow, heat transfer and associated phenomena such as chemical reactions by means of computer-based simulation" [1]. Fluid flow may be very hard to predict and differential equations that are used in fluid mechanics are difficult to solve. Technological growth, understood both as the development of powerful computers and numerical algorithms, gave the chance to solve these kind of physical problems and has made it possible to use CFD as a research and design tool.

1.2 Turbocharger fundamentals

1.2.1 Working principle

Supercharging and turbocharging are the of the most common used methods of forced gases induction. In Figure 1.1 a simple representation of the former. Turbocharged systems typically have better power and efficiency from mid to high engine operating speeds, while superchargers have good performance at low engine speeds.

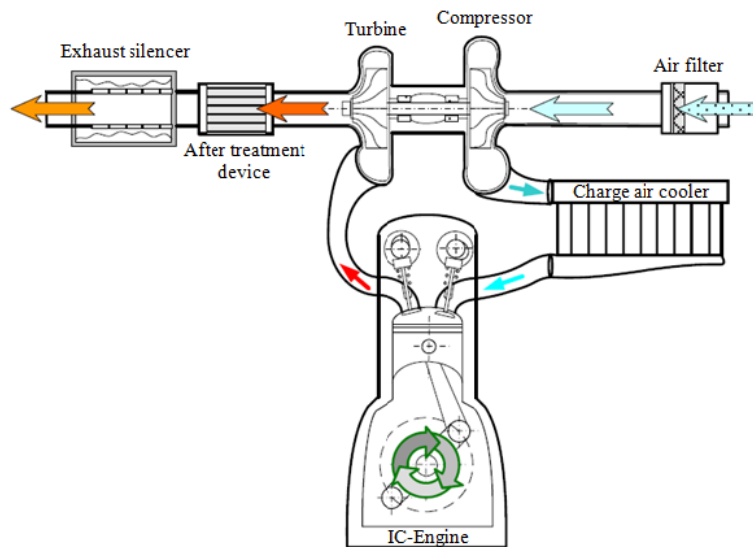


Figure 1.1: Turbocharger - Engine system schematic [2]

The main difference between supercharging and turbocharging is due to the fact that in the first case the compressor that guarantees the boost pressure is mechanically driven by the engine, typically using belts, which means that exhaust energy is not recovered, thus no efficiency increase is obtained. Hence, turbocharging is the most common used technique in today's automotive world since it allows to highly improve efficiency of the system. In high displacement engines, twin or parallel turbocharging is often employed with one turbocharger per bank of cylinders, sometimes with usage of sequential turbochargers to extend the range of operation of the engine and to reduce response time (turbo lag).

The broad application of turbochargers makes it very important to understand the multiple variations of the turbomachinery components that make up the turbocharger and its performance characteristics. Usually compressors used in turbochargers adopt a centrifugal design, as well as the turbine due to reduced pressure drop and mass flow involved in the process.

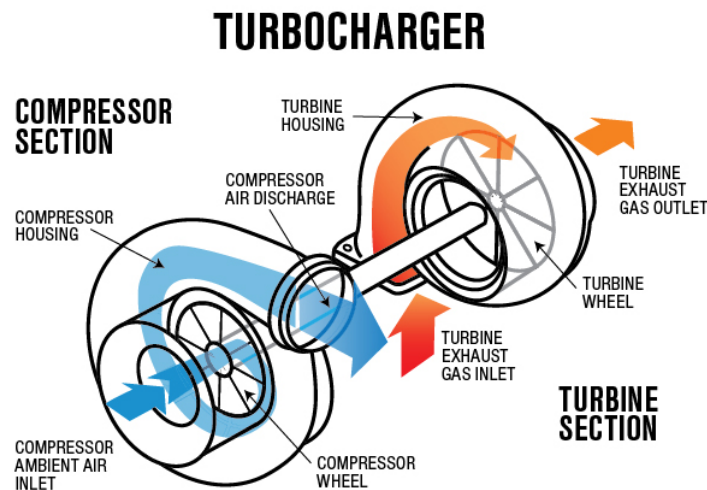


Figure 1.2: Turbocharger schematic

Figure 1.2 shows the typical configuration and flows direction in a classic automotive turbocharger. The process is powered by feeding exhaust gases from the engine exhaust manifold into the turbine housing. The heat and pressure of the exhaust gasses causes expansion of that gas: the turbine impeller extracts energy from the gasses and converts it to rotational momentum which spins the impeller. The latter is connected to a shaft which has a compressor impeller at the opposite end. Since there is a direct connection, the compressor and turbine spin at the same speed. Once the compressor starts spinning fast enough it sucks in air, compresses it, and feeds it to the engine combustion chamber.

1.2.2 Compressor side

In centrifugal compressors, air enters the housing at ambient pressure and temperature, following the characteristic helical volute is turned in the radial direction, and exits the impeller at the tip of the blade which has a larger radius than the hub. This larger radius allows the centrifugal compressor to increase the pressure higher than that of the axial compressor, which instead will require multiple stages to get same results. That is why centrifugal compressors combined with radial turbines are mostly employed for automotive application as multiple stages are not required allowing to reduce cost, space and optimization process. Following figure shows the typical performance map of a centrifugal compressor for automotive turbochargers.

On the abscissa axis the corrected mass flow rate with respect to a reference pressure and temperature is shown, on the y-axis the static outlet to total inlet pressure ratio.

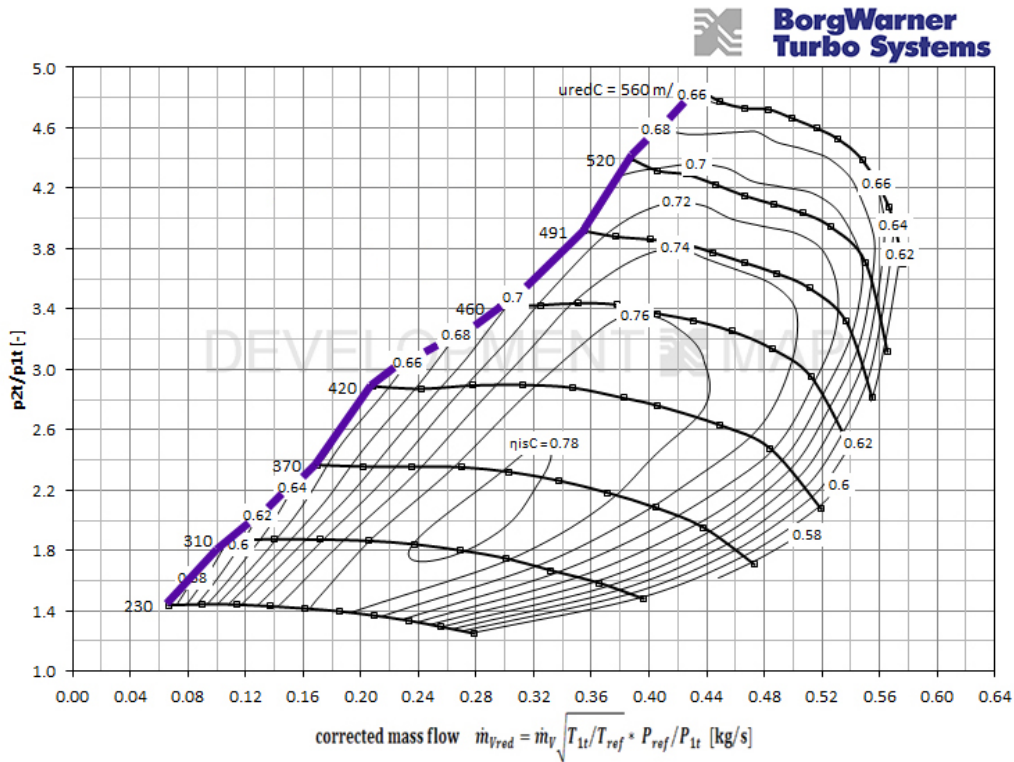


Figure 1.3: Compressor performance map [3]

The range of operation of a centrifugal compressor is usually defined by three boundaries which are the surge line to the far left, the choke line on the far right, and the over speed line at the top of the map. Therefore, designers have to make sure that the mass flow rate and pressure ratio requirements are within the range of compressor operation. In the map constant efficiency iso-entropic contours may also be noted.

1.2.3 Turbine side

As well as axial compressors realize lower boost pressure compared to centrifugal compressors, likewise axial turbines reduce the pressure less than radial turbines. This happens because all the flow manipulation happens at a constant radius on the turbine blade, whereas in a radial turbine, the flow is turned from the outer radius to the inner radius. This allows axial turbines to have a higher efficiency than radial turbines but with a smaller range of operation, therefore they are typically used for installations that tend to operate at one operating point for significant amounts of time.

In the following figures some typical radial turbines efficiency maps are reported. Figure 1.4 shows the mechanical efficiency versus the total inlet to static outlet pressure ratio, with respect

to different turbine rotational speed, labeled next to respective curves. The performance map is shown in the next figure.

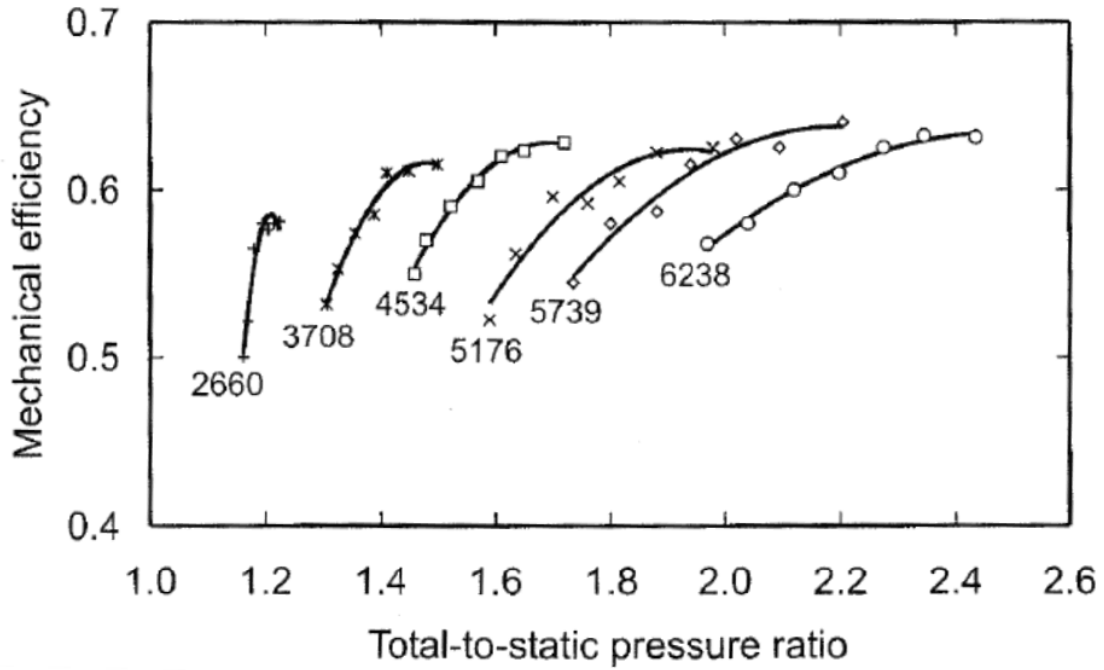


Figure 1.4: Turbine efficiency map [5]

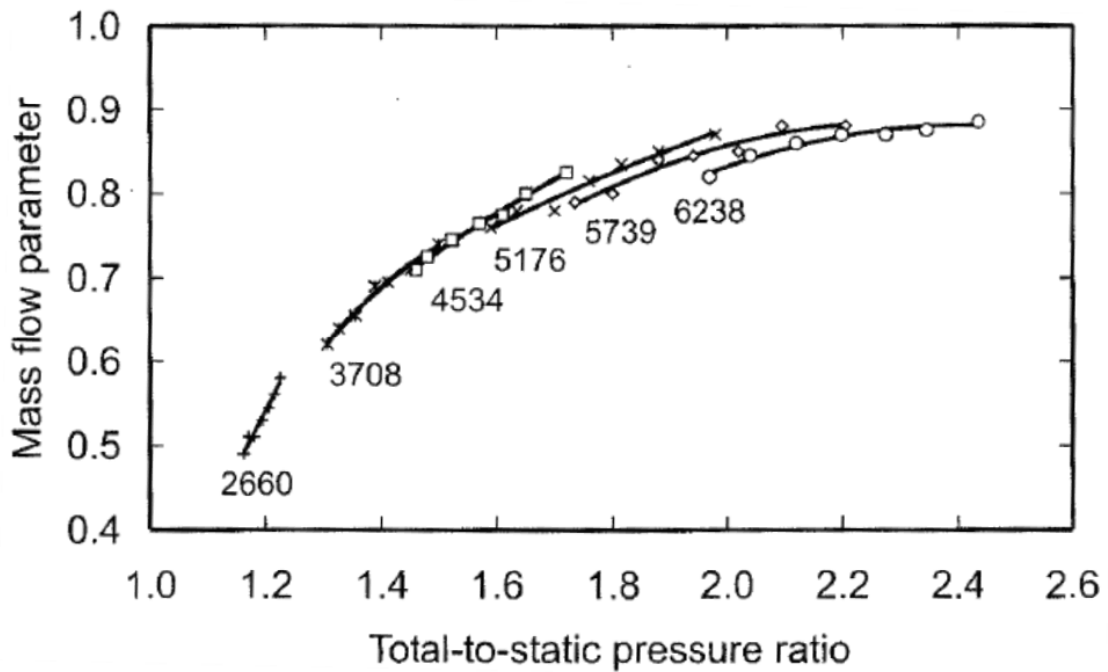


Figure 1.5: Turbine performance map [5]

During turbomatching process designers strive to obtain maximum efficiency from the energy recovery process in according to both turbine and compressor operating limits, by means of mass flow rates and pressure ratios. Moreover, designers compete to improve engine's low-end torque. In fact at low operating speeds the pressure ratio obtainable is limited by the compressor surge line which can cause instability and damage the compressor and engine themselves (cavitation phenomenon). Usual forms of failure are low cycle or thermal fatigue to the blades or pressure fluctuations concerning engine.

1.3 Turbocharging techniques

Depending on engine application, displacement and performance demand, manufacturers developed different turbochargers configuration to best suit all system requirements. Here are listed 6 typical turbocharger configurations, the review is taken from "*Melett Ltd - Wabtec Corporation*", see [4].

1. *Single turbo*

Single turbochargers are the most common solution employed for mid range cars. Completely different torque characteristics can be achieved: large turbos work better at higher loads, whilst smaller turbos can spool faster at low-end power. They are a convenient solution to increase engine performance and efficiency.

2. *Twin-turbo*

With this configuration an additional turbocharger is added to the engine, mostly in the case of high displacement motor such as V6 or V8, in which each turbo is coupled with one cylinder bank. Other solutions provide two turbos in series, known as twin sequential turbocharging: the smaller one used at low RPMs, the larger turbo at higher RPMs instead. Of course costs and complexity increase but operation range widens and turbo lag is reduced.

3. *Twin-scroll turbo*

Twin-scroll turbochargers are fed separately by different engine cylinders, therefore they require a divided-inlet turbine housing and exhaust manifold. In a conventional in-line 4 cylinder (firing order 1-3-4-2), cylinders 2 and 3 feed to one scroll of the turbo, cylinders 1 and 4 feed to another. This helps to improve efficiency of the system in terms of

generated power and reduced turbo lag, but the main drawback is the cost associated with the complexity of the turbine housing and the exhaust manifold.

4. *Variable Geometry turbo*

VGTs are one of the most common used solution amongst light commercial vehicles since they allow to obtain, along with reduced costs higher performance than single turbo layout. The turbine housing is made of a ring of aerodynamically-shaped vanes which are controlled both via pneumatic or electronic components and enable to vary the cross-sectional area of the turbine. The rack position allows to control the turbos area-to-radius (A/R) ratio in order to give high low-end torque at low RPMs, and solid power at higher revs. This results in reduced turbo lag and smoother torque band. Typically their usage is limited to diesel engine car, since exhaust gases temperature in petrol car would be much higher resulting in huge costs to realize vanes in particular heat resistant alloy.

5. *Variable twin-scroll turbo*

A VTS turbocharger combines the advantages of a twin-scroll turbo and a VGT. Using a valve the system is able to redirect the flow just to one scroll or to both if the engine requires it. The VTS turbocharger design provides a cheaper alternative to VGT turbos, suitable for petrol engine applications.

6. *Electric turbo*

In recent times manufacturers developed new technologies to answer to all the negative characteristics of conventional turbochargers, introducing turbocharger electrification. Electrical driven turbos allows to drastically reduce turbo lag and assist a normal turbocharger at lower engine speeds where a conventional turbo is not efficient. This increases the turbo operational window and enhances performance under all aspects. Again there are some disadvantages, mostly regarding cost and complexity of the system since the motor should be cooled to prevent failures. An example is BorgWarner's eBooster [3] shown in Figure 1.6. A similar version of this can be found in Audi's SQ7 [14].

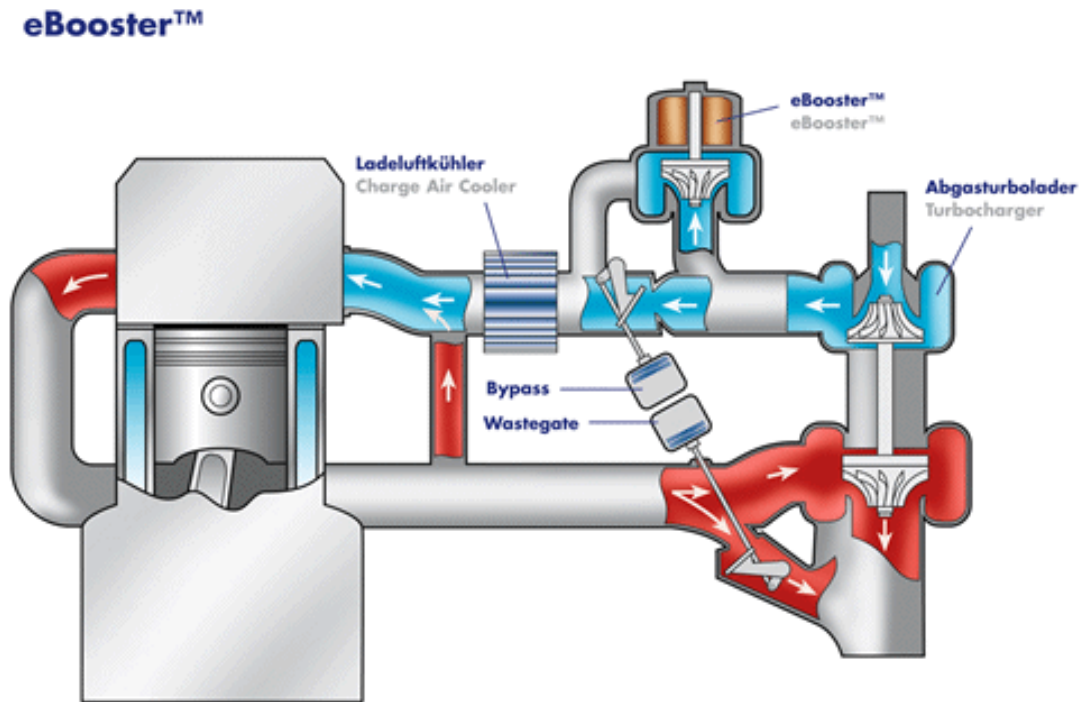


Figure 1.6: BorgWarner's eBooster scheme [3]

1.4 CFD analysis software

In the present study, CFD simulation on a radial turbocharger was conducted to analyze the impact of geometry changes on the turbine stage, using different CFD software such as SolidWorks Flow Simulation and GT-Power Suite.

The former was mainly used to carry out 3D CFD simulations to study the flow trend inside the turbine scrolls, optimize internal aerodynamics and collect data about pressure and temperature drops of the turbine volute, as well as the acceleration given to the fluid.

The latter enables to put the turbocharger inside a more complex environment, where the whole engine could be simulated. This allows more in-depth investigation about the impact of the different turbine A/R ratio over the engine performance, BSFC and efficiency, giving a wide panorama of the different working conditions.

1.4.1 SOLIDWORKS FloXpress™

The package FloXpress is a preliminary data flow analysis tool in which water or air concentrates on parts or assemblies. After defining input and boundary conditions for the model, the software roughly calculates flow trajectories, showing in particular flow's velocity. Thanks to that, it's possible to find any issues in the project and improve them before building the actual parts [8].

1.4.2 SOLIDWORKS Flow Simulation™

Flow Simulation is the next step in fluid dynamic analysis. It is a general-purpose fluid flow and heat transfer simulation tool capable of simulating both low-speed and supersonic flows. The advantages compared to the other package are considerable. Besides allowing a better control of the geometry to evaluate the correct flow path, this tool allows to define with greater accuracy the parameters of the analysis, in order to obtain very high quality results and adherent to the reality [8]. This paper takes advantage of some of them in particular, e.g the possibility of defining a rotating mesh to simulate the rotation of the impeller or the ability to define custom fluids to perform calculations, exhaust gases in this specific case.

1.4.3 GT-POWER Suite™

GT-POWER is the industry standard engine performance simulation, used to predict engine performance quantities such as power, torque, airflow, volumetric efficiency, fuel consumption, turbocharger performance and matching, and pumping losses. Beyond basic performance predictions, GT-POWER includes physical models for extending the predictions to include cylinder and tailpipe-out emissions, intake and exhaust system acoustic characteristics (level and quality), in-cylinder and pipe/manifold structure temperature, measured cylinder pressure analysis, and control system modeling [9].

Chapter 2

Literature review

The turbocharger is made up of different components: the compressor, the turbine, main housing and the shaft. The rotor of the turbocharger is supported by a bearing system which has to stand critical conditions, assuming revolution speeds up to 150k rpm. Both the turbine and compressor impellers are linked to rotating shaft, resulting in the same rotational speed.

A fundamental understanding of the flow behavior of a radial turbine is necessary to be able to properly read the results from the CFD calculation performed in this simulation.

2.1 Radial turbine theory

The design of a radial turbine can be represented by the turbine housing, the rotor and the stator. The thermodynamic process which evolve inside the component is shown in the h-s diagram of Figure 2.1 an h-s. Each point is indicative for the area that the fluid is going through at that specific moment. 0 label stands for volute inlet, 1 for nozzle inlet, 2 stator throat, 3 stator outlet, 4 rotor inlet, 5 rotor throat, 6 rotor outlet and 7 diffuser outlet. The energy recovery process, thus the mechanical power output is obtained at the rotor stage, thanks to the heat and the pressure drop granted by expanding exhaust gases. The amount of power extracted depends on the mass flow rate of the exhaust gas, the expansion ratio and the isentropic enthalpy drop in the turbine itself.

2.1.1 Governing equations

Writing the First Law of Thermodynamics for an for an infinitesimal variation of state [6]:

$$dE = dQ - dW_t \tag{2.1}$$

where

$$E = U + \frac{1}{2}mc^2 + mgz \quad (2.2)$$

If considering a steady state flow the equation 2.1 can be written as follows:

$$\dot{Q} - \dot{W}_x = \dot{m} \left[(h_7 - h_0) + \frac{1}{2}(c_7^2 - c_0^2) + g(z_7 - z_0) \right] \quad (2.3)$$

Since the height difference in these application is usually minimal the contribution from the last term $g(z_7 - z_0)$ is usually negligible and thus ignored in calculations. The other two terms are usually rewritten as the total enthalpy,

$$h_0 = h + \frac{1}{2}c^2 \quad (2.4)$$

where the gas specific enthalpy h (enthalpy per mass unit, J/kg) is defined as

$$h(T) = c_p(T - T_0) + h(T_0) \quad (2.5)$$

assuming $h(T_0) \equiv 0$ at $T = 0$ K. Thus, $h(T) = c_p T$.

Therefore, the effective turbine power results as:

$$P_T = \eta_T \dot{m}_T |\Delta h_{sT}| \quad (2.6)$$

the isentropic enthalpy drop is calculated as follows:

$$|\Delta h_{sT}| = c_{p,g} T_3 \left[1 - \left(\frac{p_4}{p_3} \right)^{\left(\frac{k}{k-1} \right)_g} \right] \quad (2.7)$$

Then combining equations 2.7 and 2.6, it's possible to obtain the effective turbine power in function of the mass flow rate, inlet temperature and pressure ratio of the turbine.

$$P_T = \eta_T P_{T,ideal} \equiv \eta_T \dot{m}_T c_{p,g} T_3 \left[1 - \left(\frac{p_4}{p_3} \right)^{\left(\frac{k}{k-1} \right)_g} \right] \quad (2.8)$$

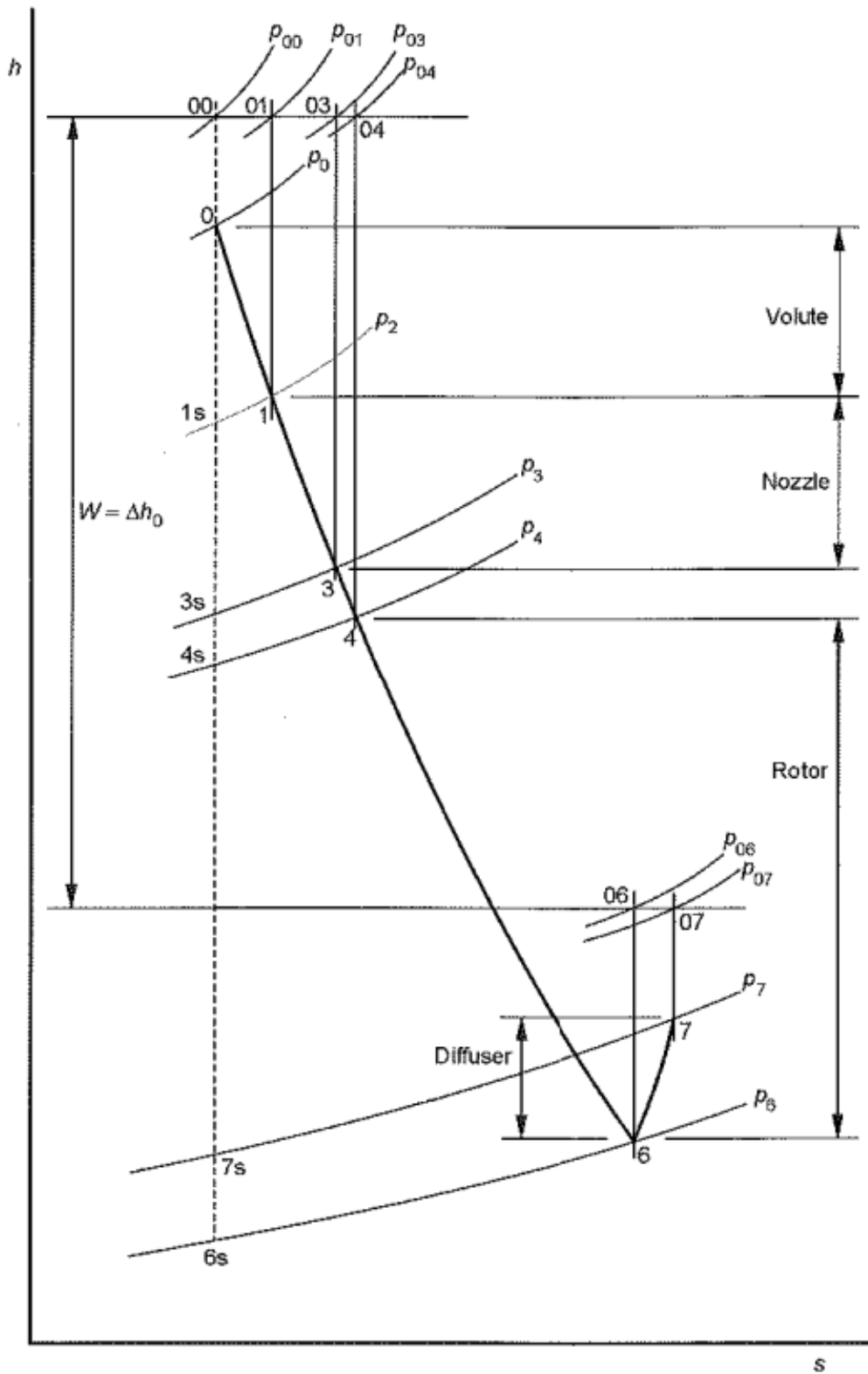


Figure 2.1: h - s diagram of the process of a radial turbine [7]

Since the support bearing system is not ideal, it causes losses due to the friction and the mechanical efficiency η_m must be considered to evaluate the absorbed power from compressor.

$$P_T = \eta_m \eta_T P_{T,ideal} = \eta_m \eta_T \dot{m}_T c_{p,g} T_3 \left[1 - \left(\frac{p_4}{p_3} \right)^{\left(\frac{k}{k-1} \right)_g} \right] \quad (2.9)$$

Likewise, it is possible to get compressor power from the isentropic drop and efficiency as follows:

$$P_C = \frac{P_{C,ideal}}{\eta_C} \equiv \frac{\dot{m}_C \Delta h_{sC}}{\eta_C} \quad (2.10)$$

Using thermodynamic equations for an isentropic process, the required compressor power is calculated:

$$P_C = \frac{\dot{m}_C c_{p,a} T_1}{\eta_C} \left[\left(\frac{p_2}{p_1} \right)^{\left(\frac{k}{k-1} \right)_a} - 1 \right] \quad (2.11)$$

The performance map of the turbine shown in Figure 2.2 displays the corrected mass flow rate over the turbine expansion ratio π_T . Over a certain pressure ratio the mass flow rate is no longer increasing which means that the flow is choked, even at higher rotational speeds. The exhaust gas speed reaches the sonic speed with Mach number $M = 1$.

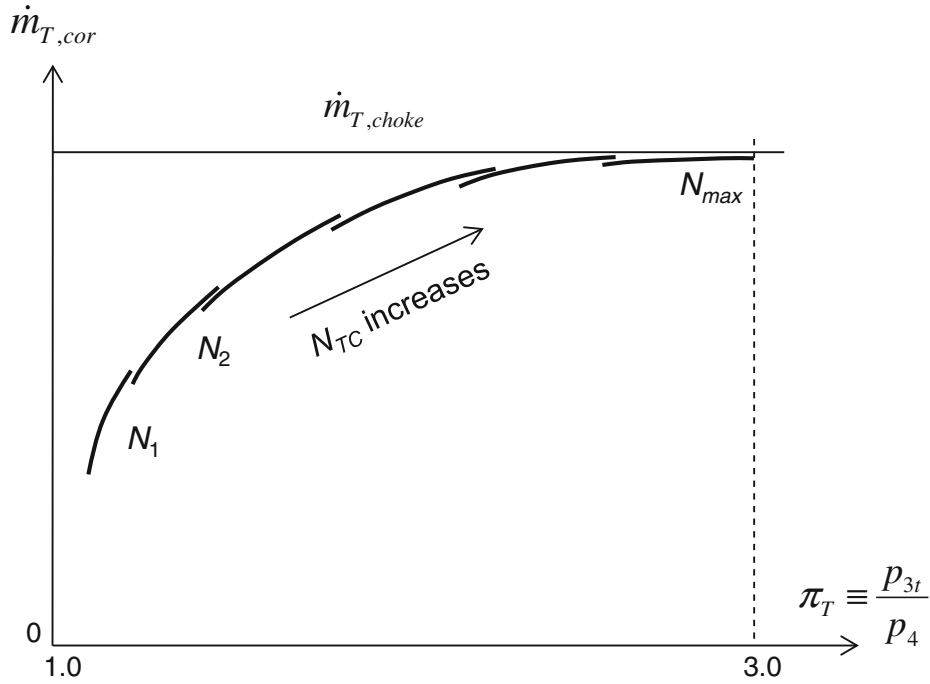


Figure 2.2: Turbine performance map [6]

2.1.2 Fluid specific work

For a turbine running at an angular velocity Ω the fluid specific work on the rotor is defined

$$\frac{\dot{W}_t}{\dot{m}} = \tau_A \Omega = (U_0 c_{\theta 0} - U_7 c_{\theta 7}) \quad (2.12)$$

where

$$\dot{W}_t = \dot{m}[h_{00} - h_{07}] \quad (2.13)$$

Equation 2.13 is called Euler's turbine equation and can be rewritten using equations 2.12 and 2.13:

$$I = h_0 - U c_\theta \quad (2.14)$$

where I is widely called rothalpy and is constant along streamlines through the turbine. By substituting relative velocity for absolute velocity the relative total enthalpy can be derived. The rothalpy is defined as

$$I = h_{0,rel} - \frac{1}{2}U^2 \quad (2.15)$$

where the relative total enthalpy is defined as

$$h_{0,rel} = h + \frac{1}{2}w^2 \quad (2.16)$$

This property is useful when analyzing the flow of a rotating system like a turbine, since the rothalpy will stay constant through the rotating stage.

A simple form of the isentropic efficiency of the turbine is defined as a function of the enthalpy:

$$\eta_i = \frac{h_{00} - h_{07}}{h_{00} - h_{07s}} \quad (2.17)$$

2.1.3 Volute

The purpose of the volute is to distribute the flow evenly to the stator blades. This is to ensure that each of the rotor blade will receive an equal amount of mass flow, i.e. the rotor blades will be evenly loaded. The flow is uniform at the volute inlet, it is assumed to come from a straight pipe. The preliminary design is based on the assumption that the angular momentum

is constant, described by the free vortex equation and the continuity equation in θ direction:

$$\begin{aligned} rC_\theta &= \text{const} \\ m_\theta &= \rho_\theta A_\theta C_\theta \end{aligned} \quad (2.18)$$

2.2 Solidworks - Computational architecture

The realization of a CFD analysis requires an accurate phase of process structuring. In fact, the results obtainable are variable depending on the validity of the models used, as well as on the robustness of the calculation methods implemented within the software. Therefore it is essential to find an optimal solution which, at the same time, guarantees reduced simulation times but a suitable accuracy for that specific task. Different equations could be used such as Reynolds Averaged Navier Stokes (RANS) for steady simulation and Unsteady Reynolds Averaged Navier Stokes (URANS) for transient.

2.2.1 Governing equations

Flow Simulation solves the Navier-Stokes equations, which are formulations of mass, momentum and energy conservation laws for fluid flows. The equations are correlated by state equations defining the type of the fluid, and by empirical dependencies of density, and thermal conductivity. A particular problem is specified from the user by the definition of its geometry, shape and initial value conditions. The conservation laws for mass, angular momentum and energy in the Cartesian coordinate system rotating with angular velocity Ω about an axis passing through the coordinate system's origin can be written in the conservation form as follows [8]:

$$\frac{\partial \rho}{\partial t} + \frac{\partial}{\partial x_i}(\rho u_i) = 0 \quad (2.19)$$

$$\frac{\partial(\rho u_i)}{\partial t} + \frac{\partial}{\partial x_j}(\rho u_i u_j) + \frac{\partial p}{\partial x_i} = \frac{\partial}{\partial x_j}(\tau_{ij} + \tau_{ij}^R) + S_i \quad i = 1, 2, 3 \quad (2.20)$$

$$\frac{\partial \rho H}{\partial t} + \frac{\partial \rho u_i H}{\partial x_j} = \frac{\partial}{\partial x_i} \left(u_j (\tau_{ij} + \tau_{ij}^R) + q_i \right) + \frac{\partial p}{\partial t} - \tau_{ij}^R \frac{\partial u_i}{\partial x_j} + \rho \varepsilon + S_i u_i + Q_H \quad (2.21)$$

where u is the fluid velocity, ρ is the fluid density, S_i is a mass-distributed external force per unit mass due to a porous media resistance, a buoyancy and the coordinate system's rotation,

i.e., $S_i = S_i^{porous} + S_i^{gravity} + S_i^{rotation}$, h is the thermal enthalpy, Q_H is a heat source or sink per unit volume, τ_{ik} is the viscous shear stress tensor, q_i is the diffusive heat flux. The subscripts are used to denote summation over the three coordinate directions. For Newtonian fluids the viscous shear stress tensor is defined as:

$$\tau_{ij} = \mu \left(\frac{\partial u_i}{\partial x_j} + \frac{\partial u_j}{\partial x_i} - \frac{2}{3} \delta_{ij} \frac{\partial u_k}{\partial x_k} \right) \quad (2.22)$$

Here δ_{ij} is the Kronecker delta function (it is equal to unity when $i = j$, and zero otherwise), and μ is the dynamic viscosity coefficient.

2.2.2 Laminar/turbulent boundary model

This type of model is typically used to define flows in near-wall regions. The model is based on the so-called Modified Wall Functions approach. This enables to characterize laminar and turbulent flows near the walls, and to describe flows transitions from one type to the other, using the Van Driest's profile instead of a logarithmic profile. If the size of the mesh cell near the wall is more than the boundary layer thickness the integral boundary layer technology is used. The model provides efficient profiles of temperature and velocity for the above mentioned conservation equations [8].

2.2.3 Mesh

"Flow Simulation computational approach is based on locally refined rectangular mesh near geometry boundaries. The mesh cells are rectangular parallelepipeds with faces orthogonal to the specified axes of the Cartesian coordinate system. However, near the boundary mesh cells are more complex. The near-boundary cells are portions of the original parallelepiped cells that cut by the geometry boundary. The curved geometry surface is approximated by set of polygons which vertexes are surface's intersection points with the cells' edges. These flat polygons cut the original parallelepiped cells. Thus, the resulting near-boundary cells are polyhedrons with both axis-oriented and arbitrary oriented plane faces in this case. The original parallelepiped cells containing boundary are split into several control volumes that are referred to only one fluid or solid medium. In the simplest case there are only two control volumes in the parallelepiped, one is solid and another is fluid" [8].

The rectangular computational domain is automatically constructed (may be changed manually), so it encloses the solid body and has the boundary planes orthogonal to the specified

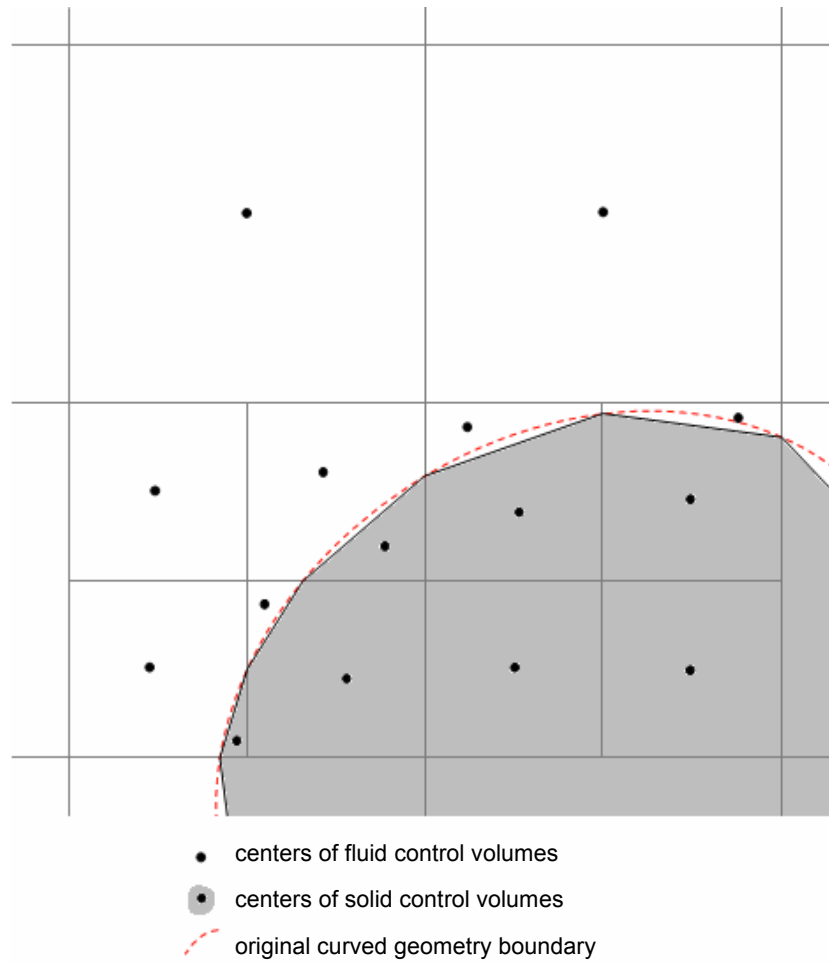


Figure 2.3: Computational mesh near the solid/fluid interface [8]

axes of the Cartesian coordinate system. Then, the computational mesh is built.

In Figure 2.4 and Table 2.1 the quality criteria for the solver is specified. The figure shows how the angle for the quadrilateral faced element is not as good as it could be. The normal vector for the integration point surface, n , and the vector that joins two control volume nodes, s , are not parallel. However for the triangular faced element the orthogonality is of highest order since the vectors are parallel. The best measurement on the mesh orthogonality is the orthogonality angle which is the area weighted average of $90^\circ - \text{acos}(n \cdot s)$. According to Table 2.1 the area weighted average of the orthogonality angle can not be smaller than 20° but local angles can be as low as 10° .

Here are described some of the criteria that the software uses to generate the mesh.

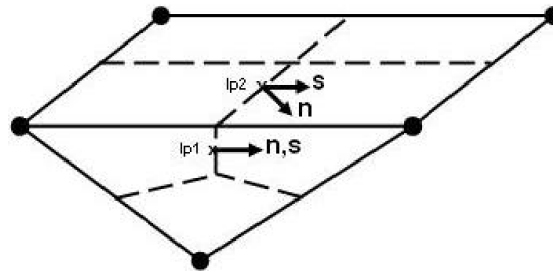


Figure 2.4: Orthogonality for quadrilateral and triangular faced elements

Measure	Acceptable range	Description
Orthogonality factor	$>20^\circ$	Area weighted average of $90^\circ - \text{acos}(n \cdot s)$
Orthogonality minimum angle	1/3	Area weighted average $n \cdot s$
Orthogonality factor	$>10^\circ$	Minimum of $n \cdot s$
Minimum and maximum face angle	$>10^\circ$ and $<170^\circ$	Minimum and maximum angle between edges of each face
Minimum and maximum dihedral angle	$>10^\circ$ and $<170^\circ$	Minimum and maximum angle between element face

Table 2.1: Solidworks Flow Simulation mesh criteria

2.3 GT-Power model implementation

Turbine and compressor performance are modeled in the software using performance maps which can be summarized as a series of performance data points, each of which describes the operating condition by speed, pressure ratio, mass flow rate, and thermodynamic efficiency. The maps are configured so that if the speed and either the mass flow or pressure ratio are known, the efficiency and either the mass flow rate or pressure ratio can be found in the map. The software predicts the turbocharger speed and the pressure ratio (PR) across turbine and/or compressor at each timestep, and therefore they are "known" with respect to the turbo map. The mass flow rate and efficiency are then looked up in the table and imposed in the solution.

2.3.1 Maps evaluation

During pre-simulation routine, 'TurbineMap' reference object is processed in GT-SUITE. The software creates a series of plots to help the user to determine the quality of data fit and interpolation. Also, they could give useful information and indicate how to modify the map data in order to improve the fit.

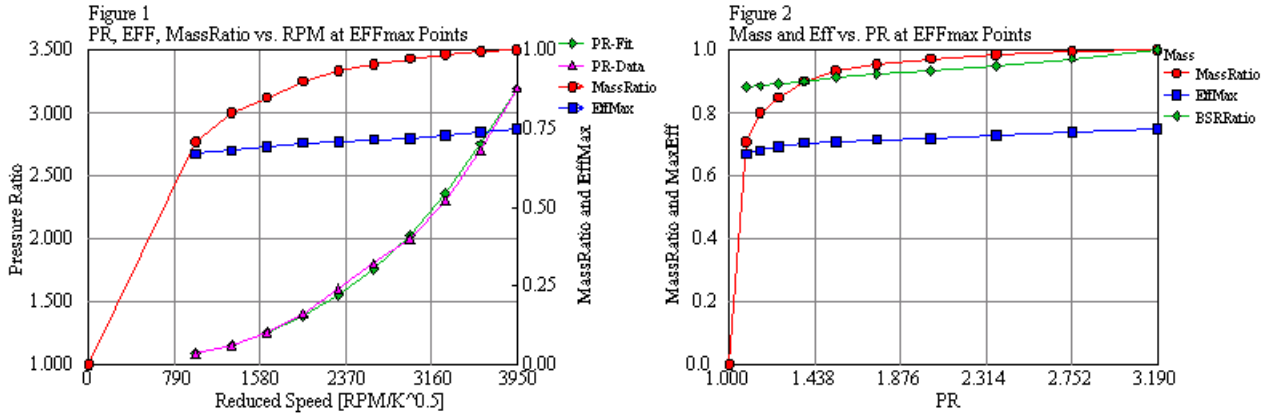


Figure 2.5: Turbine maps fitting curves, 1 [13]

Plot on the left shows the fit of the pressure ratio against the corrected speed, assuming that the Blade Speed Ratio (BSR) at these points varies linearly with pressure ratio. For a good fit the curves must be as close as possible to each other. In the same plot is possible to see the mass flow rate and maximum efficiency points fits with respect to the reduced speed. On the right, the same plots of mass flow ratio, BSR and maximum efficiency points obtained in relation to the pressure ratio.

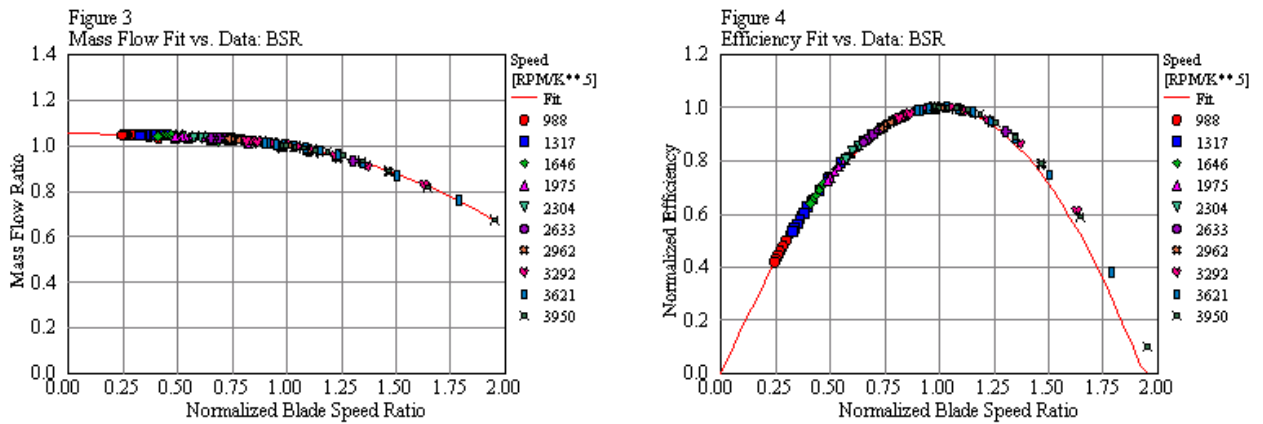


Figure 2.6: Turbine maps fitting curves, 2 [13]

The above picture on the left shows all the points regarding mass flow rate entered by the user and the curve fit created by the software. If the points lie on the curve, the interpolation obtained is fairly good and usable for simulation. Data points that do not lie on the curve indicate possible problems with those points. Basically this trend gives an indication about the goodness of the fitting process. Similar result is visible on the right where maximum efficiency points are reported over the fitting curve. Both values are plotted against the normalized blade speed ratio.

In any case, the graphs shown above are intended to make the user aware of the fitness of the inserted maps and consequently of the results obtained from the simulations. Usually one of the most common problems which can be identified thanks to these plots concerns *Outliers*: isolated points which don't follow the fitting curve suggested by the software. These bad values can be easily identified and eventually removed from the map by visual examination of the trends.

Consideration for Variable Geometry Turbines

VGTs are simulated with several maps, one for each rack position that are fit independently. Specific calculated values by GT-Power for a map do not take into account the constants of the neighboring maps. This may result in a non-linear turbine performance, and in particular the oscillation might be very bad when the rack position is adjusted to control a performance target, e.g. boost pressure, causing solution instability and never converging on the target. So particular attention must be given to these aspects.

Chapter 3

Model description

The model used for the simulations refers to a Garrett 3 Series (GT3) Turbocharger, engaged for medium size engines with displacement of 1.8 - 3.0L. Below is a quick review of the model and the changes that have been made to perform valid simulations.

3.1 Geometry overview

In Figures 3.1 - 3.2 a general view of the turbocharger and a front section are shown, in which it is possible to appreciate all the internal components and the building structure.

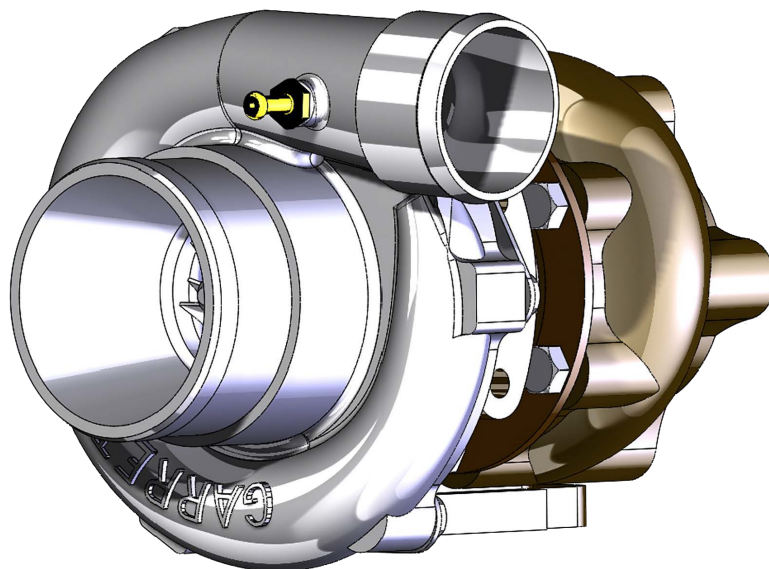


Figure 3.1: Turbocharger model

In particular, the study focused on the analysis of the turbine's housing, whose main technical specifications are now reviewed in order to obtain a clear vision of the model used.

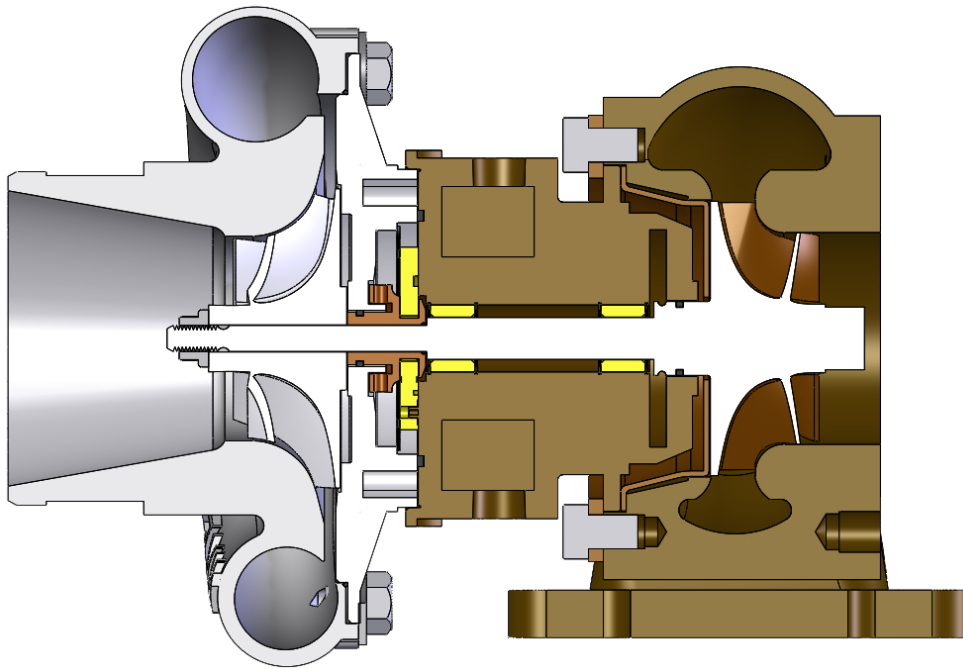


Figure 3.2: Turbocharger front section

3.1.1 Wheel's trim

To describe a turbocharger some parameters are essential to define its characteristics. The wheel's trim expresses the relationship between the inducer and exducer of both turbine and compressor wheels. More accurately, it is an area ratio. The inducer diameter is defined as the diameter where the air enters the wheel, whereas the exducer diameter is defined as the diameter where the air exits the wheel [10].

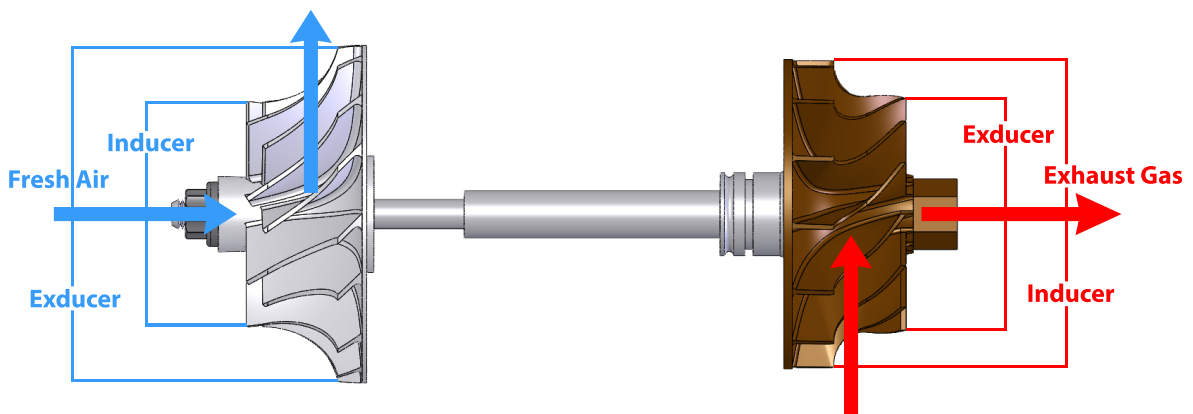


Figure 3.3: Inducer / Exducer for turbine and compressor's wheel

Based on aerodynamics and air entry paths, the inducer for a compressor wheel is the smaller diameter. For turbine wheels, the inducer it is the larger diameter, see Figure 3.3.

Wheel's trim, can be calculated in the following way, (measurements in calculations are expressed in mm):

$$Trim = \left(\frac{Inducer^2}{Exducer^2} \right) \cdot 100 \quad (3.1)$$

Compressor's trim

$$Trim, C = \left(\frac{47^2}{70^2} \right) \cdot 100 = 45 \quad (3.2)$$

Turbine's trim

$$Trim, T = \left(\frac{52^2}{60^2} \right) \cdot 100 = 75 \quad (3.3)$$

3.1.2 Turbine housing A/R

A/R (Area/Radius) describes a geometric characteristic of all compressor and turbine housings. Technically, it is defined as: the inlet (or, for compressor housings, the discharge) cross-sectional area divided by the radius from the turbo centerline to the centroid of that area, as shown in Figure 3.4. The A/R parameter has different effects on the compressor and turbine performance, as outlined below.

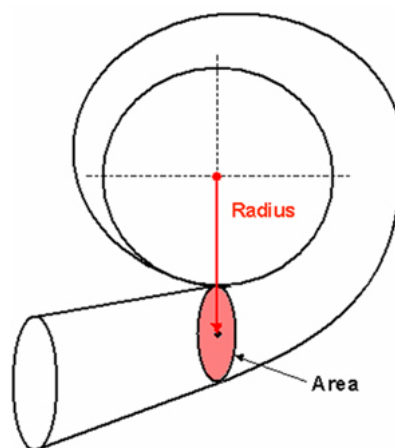


Figure 3.4: A/R compressor illustration [10]

Turbine performance is greatly affected by changing the A/R of the housing, as it is used to adjust the flow capacity of the turbine. Using a smaller A/R will increase the exhaust gas

velocity into the turbine wheel. This provides increased turbine power at lower engine speeds, resulting in a quicker boost rise. However, a small A/R also causes the flow to enter the wheel more tangentially, which reduces the ultimate flow capacity of the turbine wheel, which will tend to increase exhaust backpressure and hence reduce the engine's ability to "breathe" effectively at high RPM, adversely affecting peak engine power.

Conversely, using a larger A/R will lower exhaust gas velocity, and delay boost rise. The flow in a larger A/R housing enters the wheel in a more radial fashion, increasing the wheel's effective flow capacity, resulting in lower backpressure and better power at higher engine speeds.

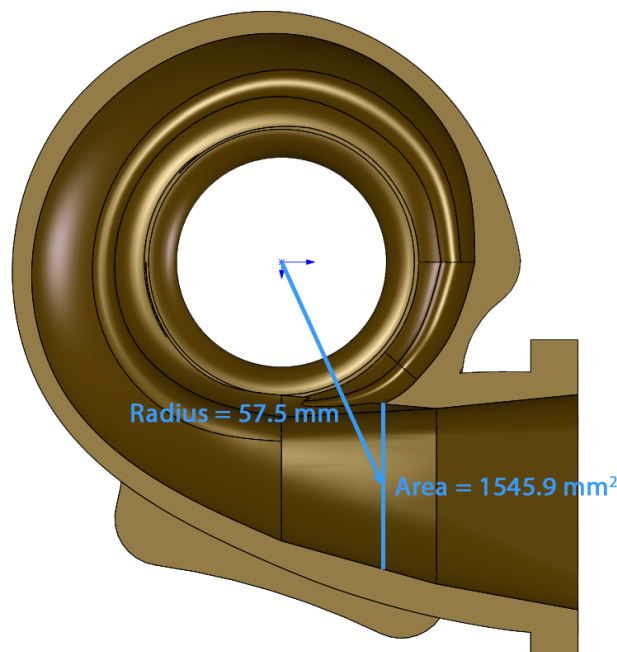


Figure 3.5: A/R turbine housing illustration

For the model under investigation, the A/R ratio is calculated as follows (also see Figure 3.5 for reference):

$$\begin{aligned} A/R &= \frac{1545.9}{57.5} = 26.9 \text{ mm} \\ &= 1.06 \text{ inches} \end{aligned} \tag{3.4}$$

3.2 Reference data

The model being studied refers, both for performance and geometry, to an existing model of turbocharger realized by Honeywell Garnett®. This belongs to the 3 series and in particular the GT3071R model, of which the experimental data will be used to validate the model and make comparisons for different working conditions.

Of particular interest for the simulations developed in this paper, is the turbine exhaust flow chart of the turbocharger, available in the official catalogue and shown below, Figure 3.6.

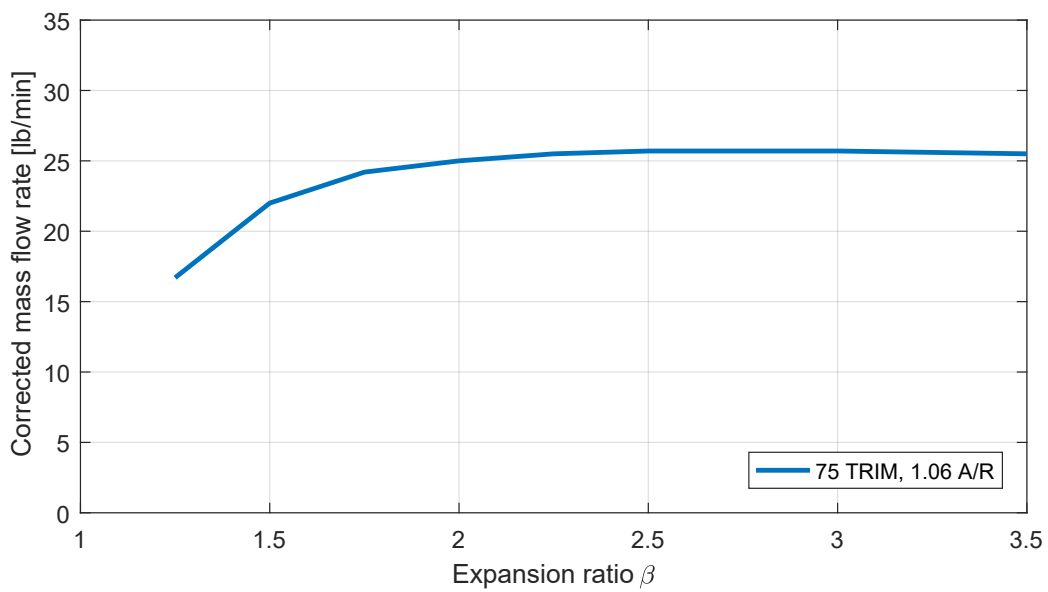


Figure 3.6: Exhaust gas flow chart - Garrett GT3071R [10]

Chapter 4

SolidWorks simulation setup

4.1 Computational domain creation

In order to perform valid simulations, it is necessary to prepare the model according to the specific software requirements. In particular, in the following study, the behavior of the fluid inside the volute of the turbine housing is analyzed, for which it's crucial to isolate this particular domain.

To do that, two different tasks were performed: the inlet was closed using the *Create Lids* option present in SolidWorks, while the outlet, represented by the cylindrical surface at the inlet for the impeller, was sealed by extruding some material around the surface itself, see Figure 4.1 below.

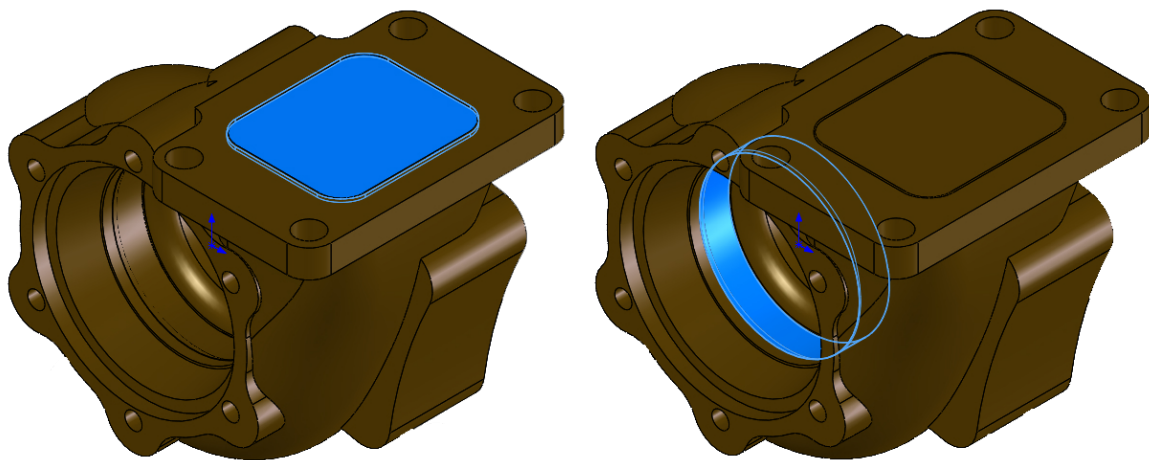


Figure 4.1: Lids' creation to isolate volute domain

4.1.1 Fluid check

To make sure that these operations have been carried out correctly, it is possible to quickly check the fluid volume of the domain, as shown in the Figure 4.2.

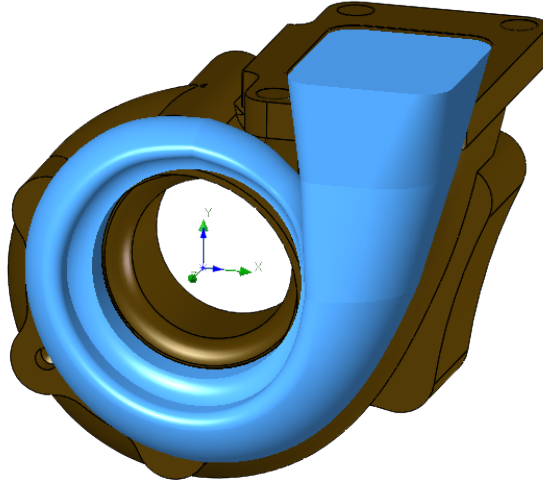


Figure 4.2: Fluid domain

4.2 FloXpress pre-analysis

The SolidWorks simulation package offers the possibility to perform preliminary analysis on the component, to validate the model and to obtain a comparison for the actual simulation. In fact, this instrument offers only an overview of how the fluid passes into the model, without providing too much details. Further studies are necessary to get a good view of the behavior of the fluid inside the model. To setup the simulation the following steps are necessary:

1. Select the type of fluid that flows inside the domain: air in the specific case;
2. Specify inlet boundary condition:
 - Type: inlet mass flow
 - $T = 843.2 K$
 - $\dot{m} = 0.197 kg/s$

3. Specify outlet boundary condition:

- Type: static pressure
- $p = 220000 \text{ Pa}$

4. Solve the model.

4.2.1 Result

As can be seen in the Figure 4.3 below, the model behaves as expected, accelerating the fluid from the inlet to the outlet of the housing turbine before the impeller. The velocity is the only information that this tool provides, which ranges from approximately 60 to 290 m/s.

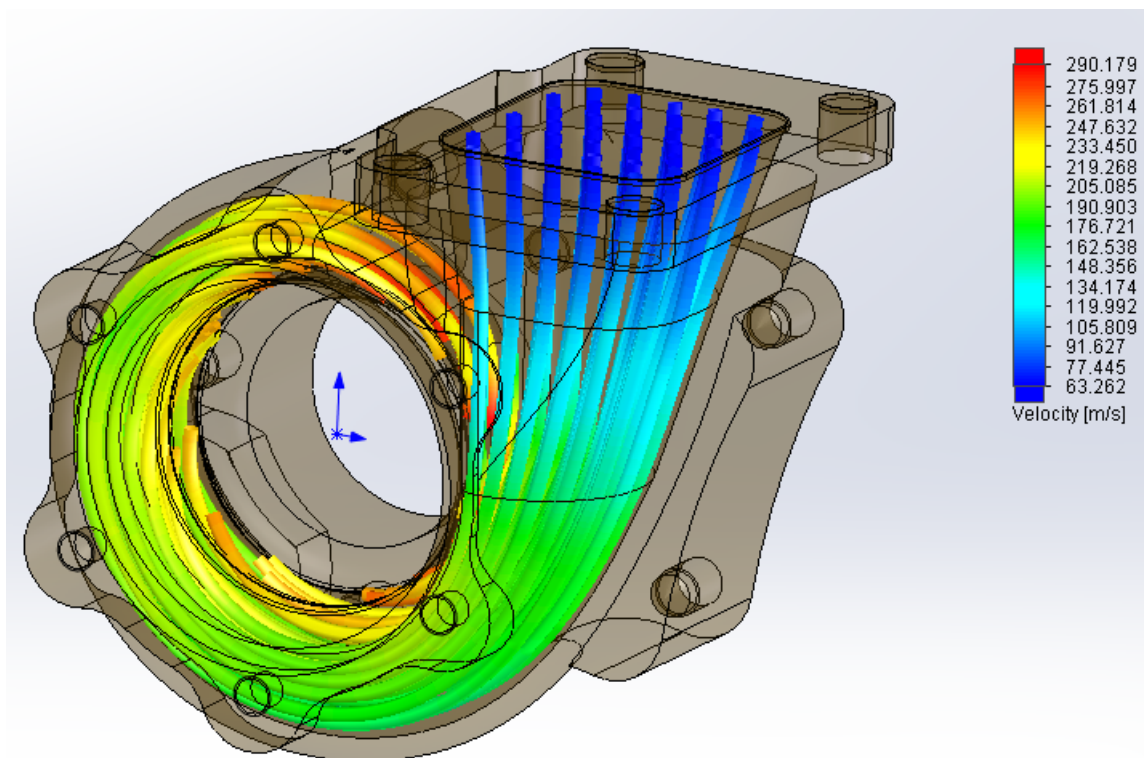


Figure 4.3: FloXpress fluid simulation result

4.3 Flow Simulation

Through this tool it is possible to carry out more in-depth investigations and go into more detail regarding the study of the flow, as well as the possibility of obtaining a greater number of results and outcomes. In fact, it is possible to obtain information on pressure, speed, temperature, enthalpy and Mach number thanks to the resolution of the NS and basic thermodynamics equations implemented by the software and discussed in Chapter 2.

Obviously this type of analysis requires a more detailed preparation and setup of the model, choosing from the type of simulation that one intends to carry out, e.g., internal, external, static or dynamic up to the type of fluid that intended to study, such as air or in the specific case exhaust gases. As previously done, it is necessary to first isolate the fluid domain and then define the type of simulation to be carried out (tasks described in paragraphs 4.1 and 4.1.1).

4.3.1 Analysis type

Since the purpose of the study is analyzing the evolution of the fluid inside the volute of the turbine housing, it is necessary to choose as type of analysis *Internal*, leaving other options as default, as shown in picture below.

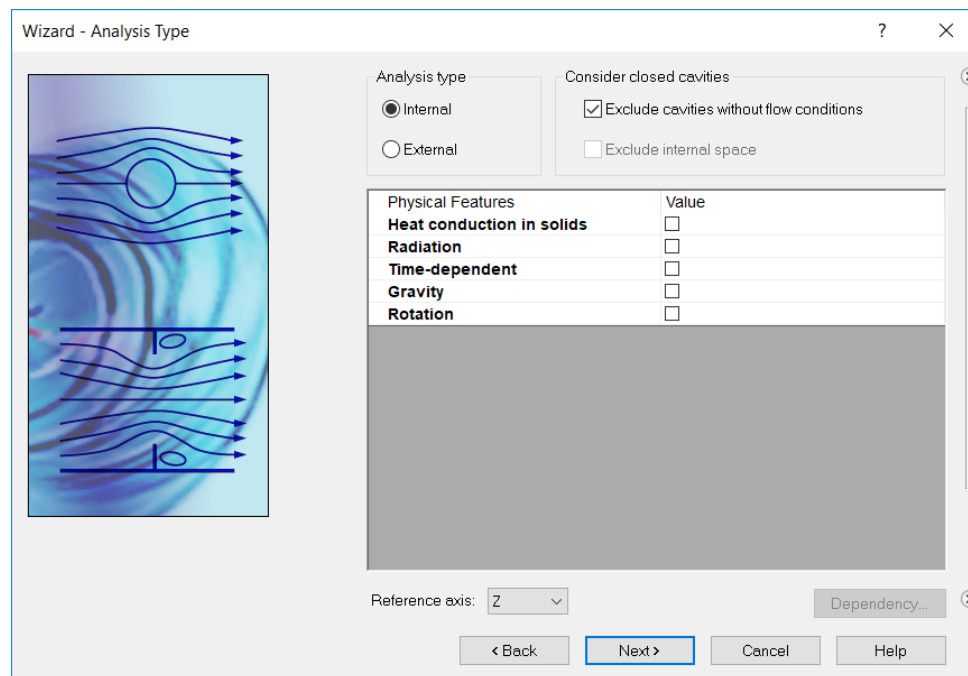


Figure 4.4: SolidWorks Flow Simulation analysis setup

4.3.2 Fluid

Simulations were conducted considering two types of different fluids: in the first instance, air was used (already present in software's presets), secondly, for a more in-depth analysis, the exhaust gas were implemented.

SolidWorks Flow Simulation allows to manually insert new fluids defined by the user through tables representing the thermodynamic properties of the same. This can be done using the *Engineering Database* available in the software, and shown below.

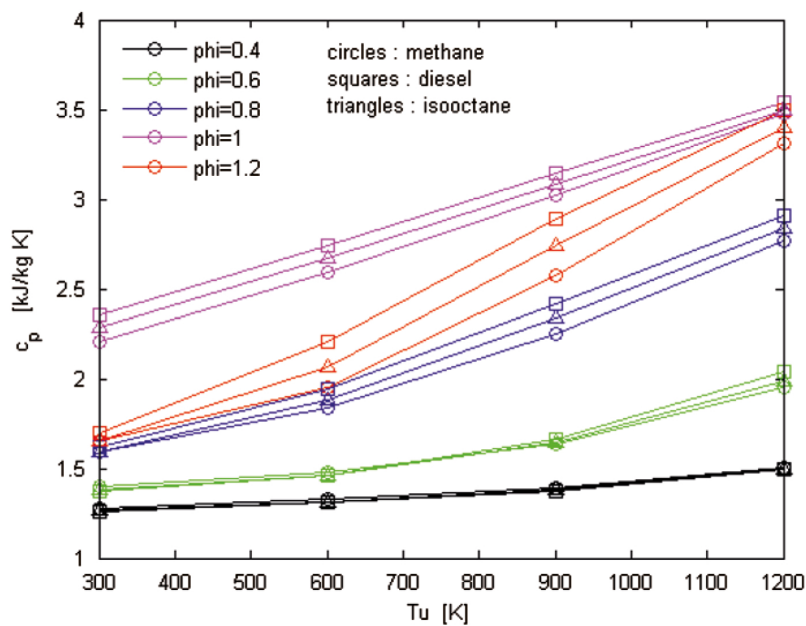
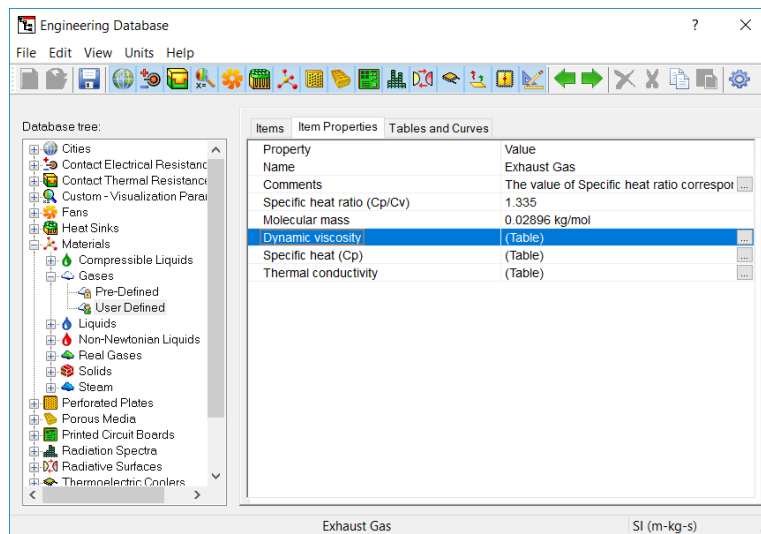


Figure 4.5: Engineering Database exhaust gas implementation [11]

Values such as the *Specific Heat Ratio* or the *Molecular mass* can be defined as a singular input; others like *Dynamic viscosity*, *Specific heat* or *Thermal conductivity* are defined using look-up tables or specific charts (Figure 4.5). In particular $k = \frac{c_p}{c_v} = 1.335 \text{ kJ/kgK}$ while the molecular mass $m = 0.02896 \text{ kg/mol}$.

4.3.3 Wall and initial conditions

As regards this setting, the software allows to set two different parameters: *Default wall thermal condition* and *Roughness*.

Default wall thermal condition

In this case it is possible to choose between different options: *Adiabatic wall*, *Heat flux*, *Heat transfer rate*, *Wall temperature*.

As part of this simulation, the first and last options were used so that a comparison of results can be made.

Roughness

Here it is possible to set the roughness of the surfaces touched by the fluid and expressed in micrometers. Even in this case the value will be changed in order to present a greater overview of results and working conditions.

Initial conditions

As well as described in the other paragraphs, here it is also possible to set the initial conditions of the fluid, such as its pressure and temperature or the input speed.

4.3.4 Computational domain and mesh

As next step, the software automatically evaluates the existence and calculation domain of the fluid, taking into account for this task the closures that were previously created.

Subsequently, the software realizes the mesh for the domain using the criteria previously described in paragraph 2.2.3. Considering the rather complex geometry of the model, consisting of accentuated and non-regular curvatures, different levels of mesh were used to perform the calculation in order to refine the results more and more and trying to reach a stable output condition.

In this phase it is therefore possible to choose different setup parameters for the mesh including:

- Level of initial mesh (ranges from 1 to 7, the higher the smaller cells);

- Minimum gap size;
- Number of cells in each x, y, z directions;
- Advanced channel refinement option.

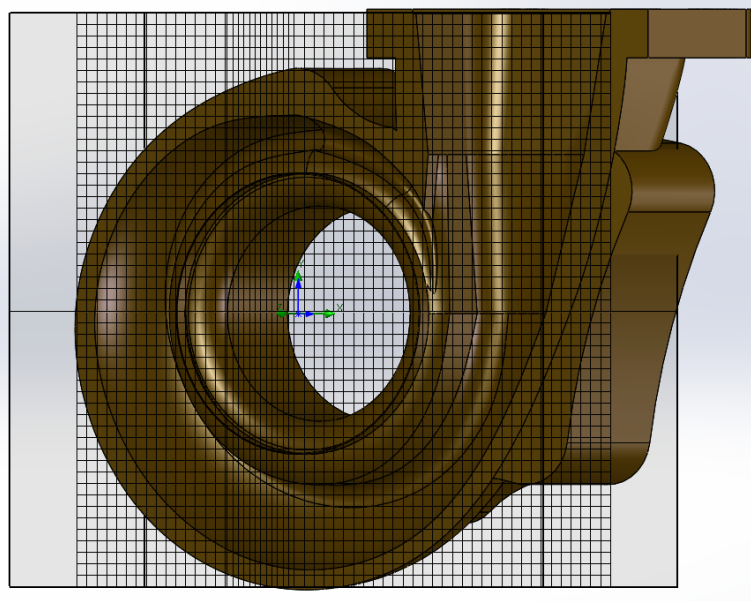


Figure 4.6: Mesh and Computational Domain visualization

4.3.5 Boundary conditions

In the model under investigation, two main BC's have been set in order to perform calculations:

A *pressure opening boundary condition*, which can be static pressure, or total pressure, or environment pressure is imposed in the general case when the flow direction and/or magnitude at the model opening are not known a priori, so they are to be calculated as part of the solution. Which of these parameters is specified depends on which one of them is known.

A *flow opening boundary condition* is imposed when dynamic flow properties (i.e., the flow direction and mass/volume flow rate or velocity/Mach number) are known at the opening. If the flow enters the model, then the inlet temperature, fluid mixture composition and turbulence parameters must be specified also. The pressure at the opening will be determined as part of the solution.

The boundary conditions need to be set in such a way that the mass flow rate and pressure ratio would not be hindered. Accordingly, an *Inlet Mass Flow* has been set at the inlet of the

turbine housing, while a *Static Pressure* at the outlet (inlet for the impeller of the turbine). See paragraph 3.2 for data reference.

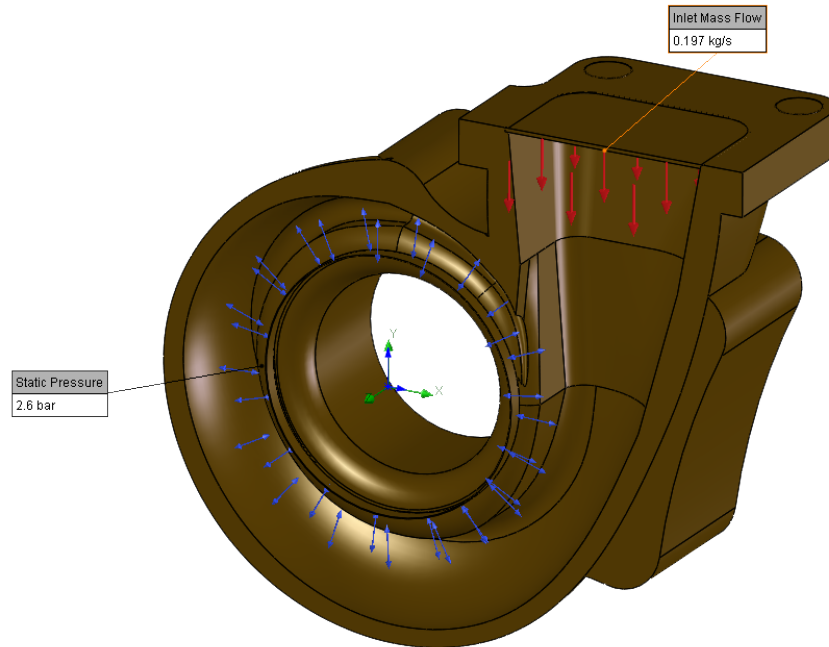


Figure 4.7: Boundary conditions setup

4.3.6 Goals & convergence

To control the calculation is important to set up some Engineering Goals in order to obtain useful data and ensure that results are accurate. Once goals are defined, the solver will check the value obtained for those parameters and compare them with the results from a previous iteration. The discrepancy of the data will determine if there's convergence or not.

Some of the value used to control the convergence are as follows:

- Inlet average temperature;
- Inlet average pressure;
- Inlet average density;
- Outlet average temperature;
- Outlet average total pressure;
- Outlet average mass flow rate.

Chapter 5

SolidWorks - Calculations

5.1 Methodology

As previously described in paragraph 3.2, the data used for the simulation is taken from an existing turbocharger model that is part of the Honeywell Garrett 3 series. The working point used to analyze the flow inside the housing turbine is shown below in the Figure 5.1.

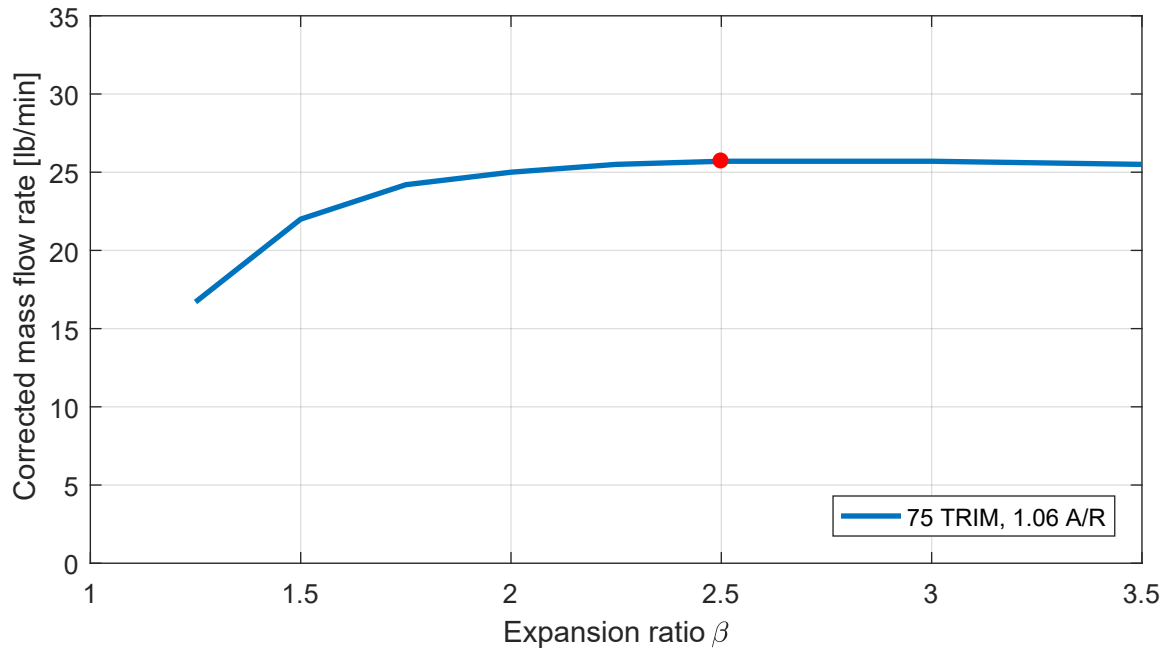


Figure 5.1: Exhaust gas flow chart - Working point

For that specific point, the working condition, such as pressure and mass flow rate, are as follows:

- Pressure ratio: $\beta = 2.5$
- Mass flow: $\dot{m} = 26 \text{ lb/min} = 0.197 \text{ kg/s}$

Since the simulations carried out do not involve the turbine impeller, but only the volute that has the task of accelerating the exhaust gases, converting part of the energy of pressure into kinetic energy, the objective to achieve was that of finding the pressure and the average speed of the fluid at the turbine housing inlet, in order to develop that specific expansion ratio.

The turbine expansion ratio β is defined as the ratio between the pressure at the inlet of the turbine housing (p_3) and the pressure at the output of the impeller (p_4). Therefore, considering a value of $p_4 \simeq 115000 \text{ Pa}$ (1.15 bar), the pressure at the inlet of the turbine housing must be equal to $p_3 \simeq 285000 \text{ Pa}$ (2.85 bar).

$$\beta = \frac{p_3}{p_4} = 2.5 \quad \rightarrow \quad p_3 = \beta \cdot p_4 \simeq 285000 \text{ Pa} = 2.85 \text{ bar} \quad (5.1)$$

5.2 Results

To achieve this result, different working conditions were simulated, gradually changing the pressure at the inlet of the impeller until the desired result is gained. With this setting, the software calculates for subsequent iterations the inlet pressure in the turbine, solving the equations discussed in Chapter 2.

Pressure	Impeller inlet [Pa]	Turbine housing inlet [Pa]
#1	$2.00 \cdot 10^5$	$2.24 \cdot 10^5$
#2	$2.10 \cdot 10^5$	$2.33 \cdot 10^5$
#3	$2.25 \cdot 10^5$	$2.47 \cdot 10^5$
#4	$2.40 \cdot 10^5$	$2.60 \cdot 10^5$
#5	$2.60 \cdot 10^5$	$2.85 \cdot 10^5$

Table 5.1: Pressures iteration at domain's boundary

Once found the correct pressure that guarantees the expansion ratio, it is possible to set

the boundary conditions (as shown in Figure 5.2) and proceed with the calculations of other parameters.

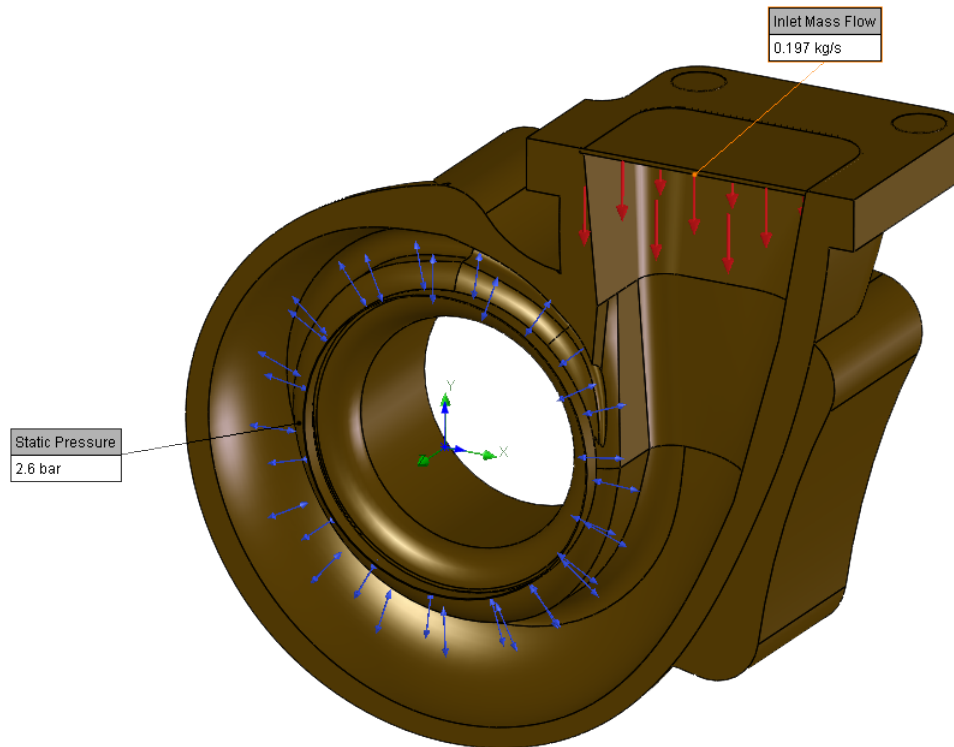


Figure 5.2: Boundary conditions setup

- *Turbine housing inlet:* Inlet mass flow, $\dot{m} = 0.197 \text{ kg/s}$ 285000 Pa, $T = 823 \text{ K} = 550 \text{ }^\circ\text{C}$;
- *Impeller inlet:* Static pressure, $p = 260000 \text{ Pa}$.

Then, simulations have been gradually refined, increasing step by step the mesh parameter, thus reducing the size of the element and improving the accuracy of the results, which are presented below by differentiating the two types of fluid used.

5.2.1 Fluid - Air

The results achieved using the software preset *Air* are quite good, however it is advisable to use the data of the exhaust gases for greater accuracy even if a certain variance of the data is always present. The results are shown in charts below.

As it is visible from the graphs as the mesh is refined, the results tend to stabilize and converge.

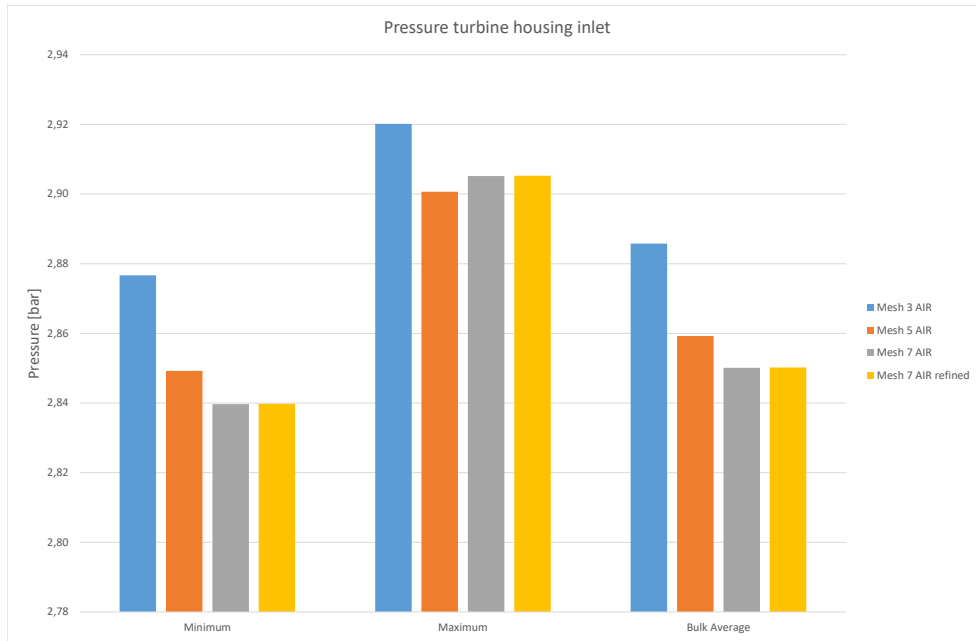


Figure 5.3: Pressure results using Air as simulation fluid

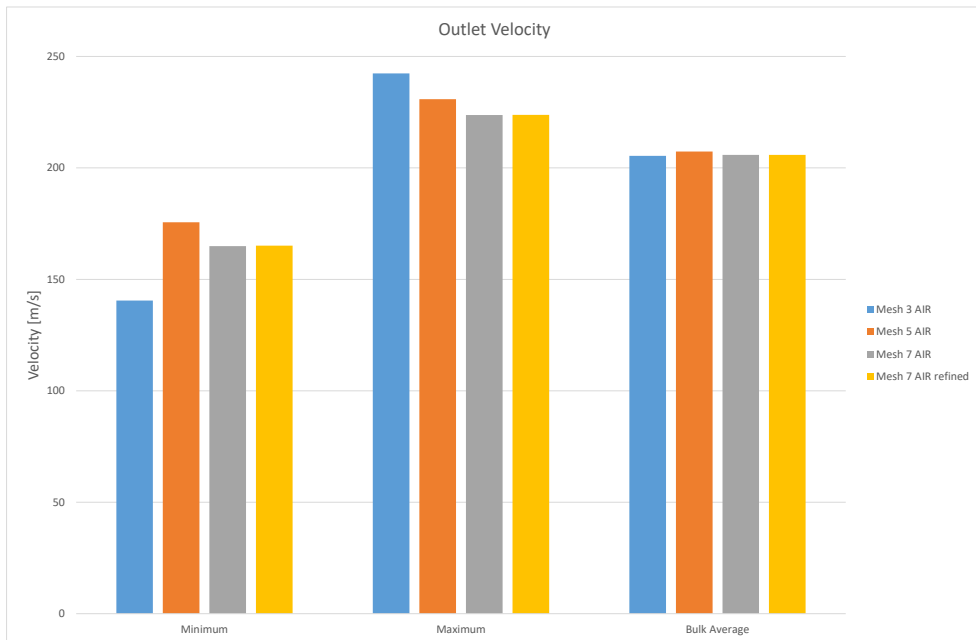


Figure 5.4: Velocity results using Air as simulation fluid

Taking as reference the bulk average value, which turns out to be the most significant, the following values are obtained:

- *Pressure at turbine housing inlet:* $2.85 \cdot 10^5 \text{ Pa} = 2.85 \text{ bar}$, which is consistent with value obtained with the previous calculations;
- *Outlet velocity:* $\simeq 206 \text{ m/s}$. The software also calculated the velocity at the inlet of the turbine housing in $\simeq 55.5 \text{ m/s}$

5.2.2 Fluid - Exhaust gas

Compared to the composition of air, the diesel exhaust gas contains increased concentrations of water vapor and carbon dioxide, the main combustion products. The concentrations of both H_2O and CO_2 can vary from a few percent, up to about 12% in diesel exhaust. These combustion products displace oxygen, the concentration of which can vary from a few percent, up to about 17% (compared to 21% in ambient air). The main component of diesel exhaust, just as is the case with ambient air, is nitrogen (N_2).

The results obtained using the exhaust gases present slightly discrepancy from those obtained using air. That is not so evident, but considering that it is the actual working fluid it is interesting to see the variation of the results.

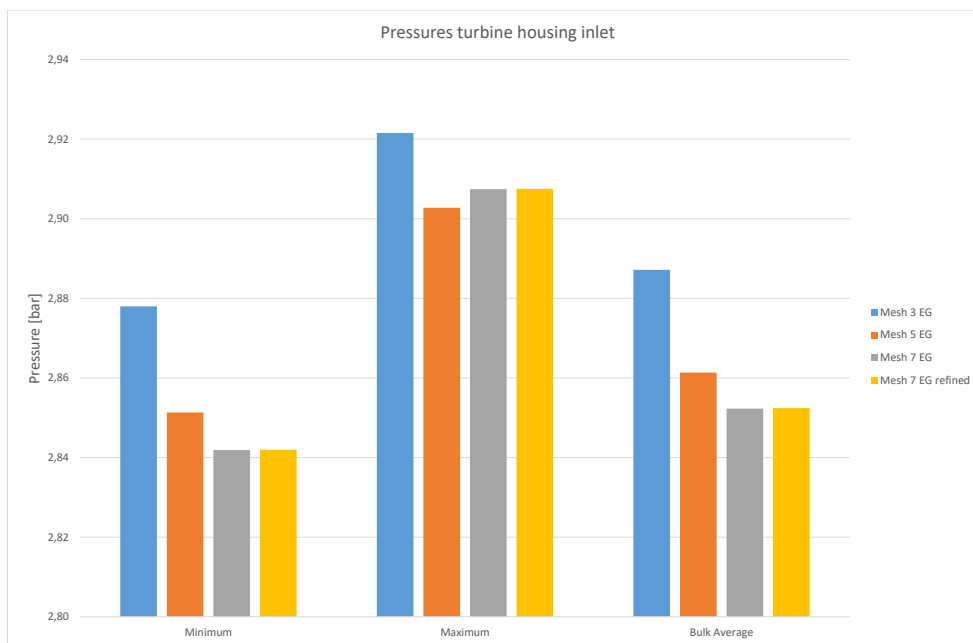


Figure 5.5: Pressure results using Exhaust gas as simulation fluid

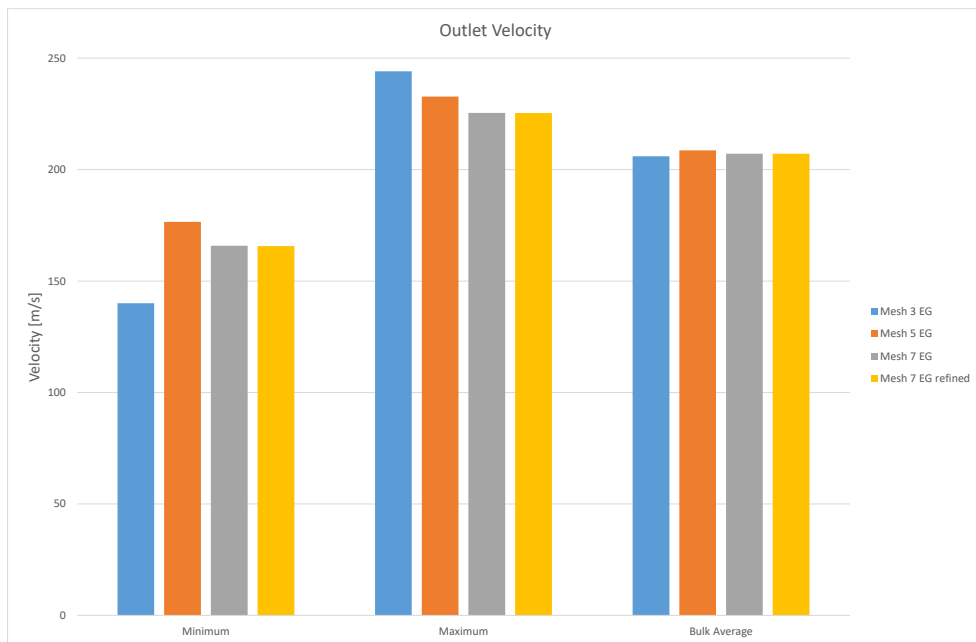


Figure 5.6: Velocity results using Exhaust gas as simulation fluid

Also in that case, taking as reference the bulk average value, the following values are obtained:

- *Pressure at turbine housing inlet:* $2.855 \cdot 10^5 \text{ Pa} = 2.855 \text{ bar}$;
- *Outlet velocity:* $\simeq 209 \text{ m/s}$.

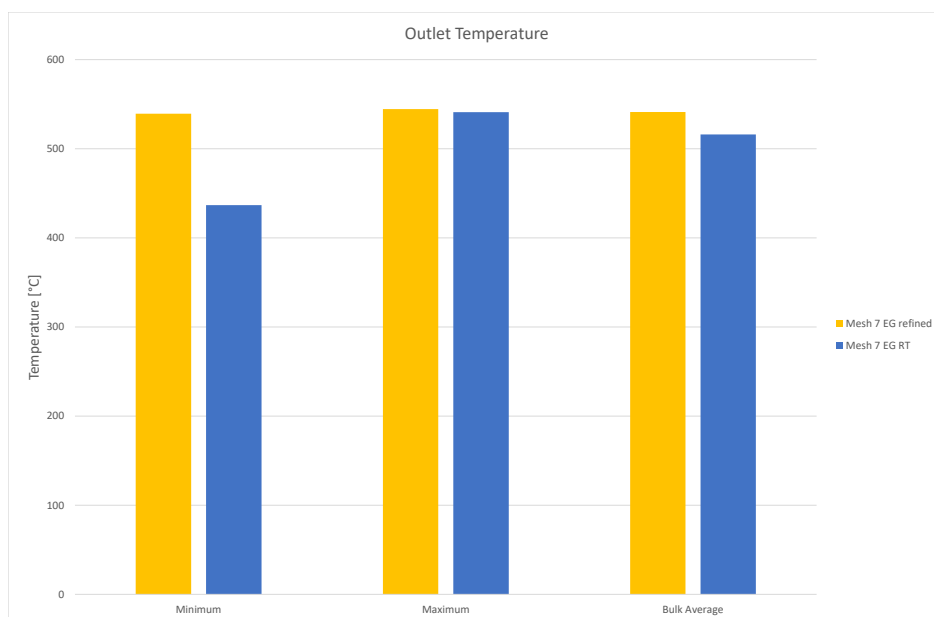


Figure 5.7: Temperature drop using a non-adiabatic system

Wall temperature Until now the calculations have been made considering the system as adiabatic, setting the *Adiabatic wall* parameter during the simulation setup. For comparison above (Figure 5.7) is shown the temperature drop obtained by considering a non-adiabatic system, with a wall temperature of 60 °C.

Analyzing the data, the variations are in some cases significant with differences in percentages ranging from 19% for the minimum temperature reached by the fluid, up to a reduced 4% for the bulk average.

5.3 Plots

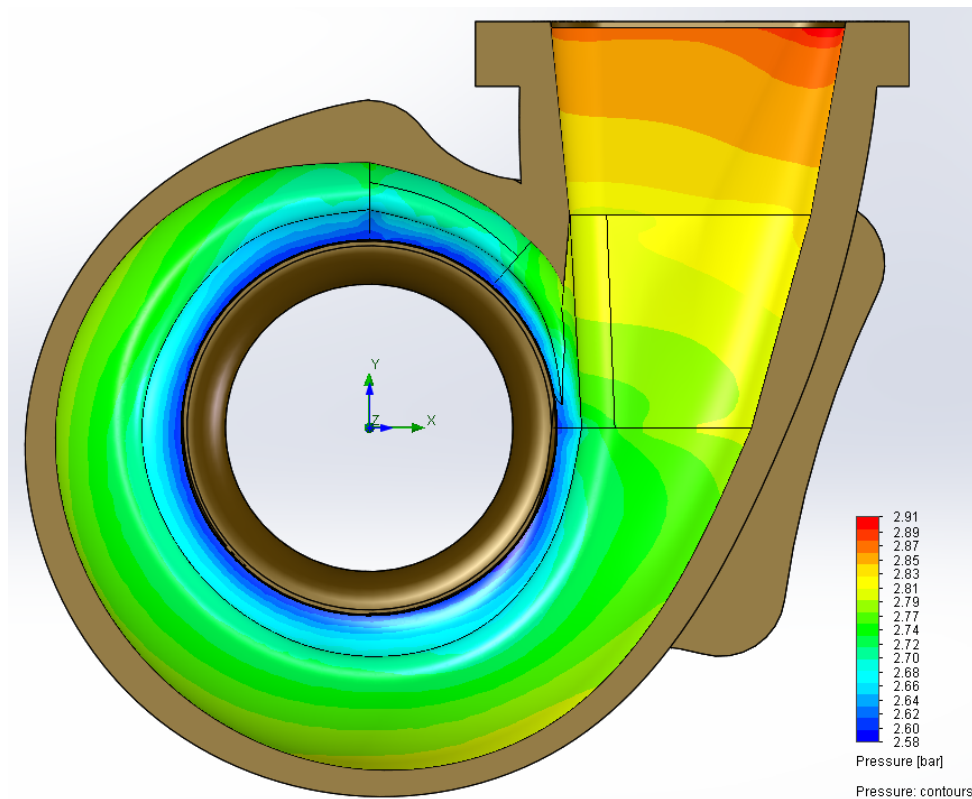


Figure 5.8: Pressure contour plot

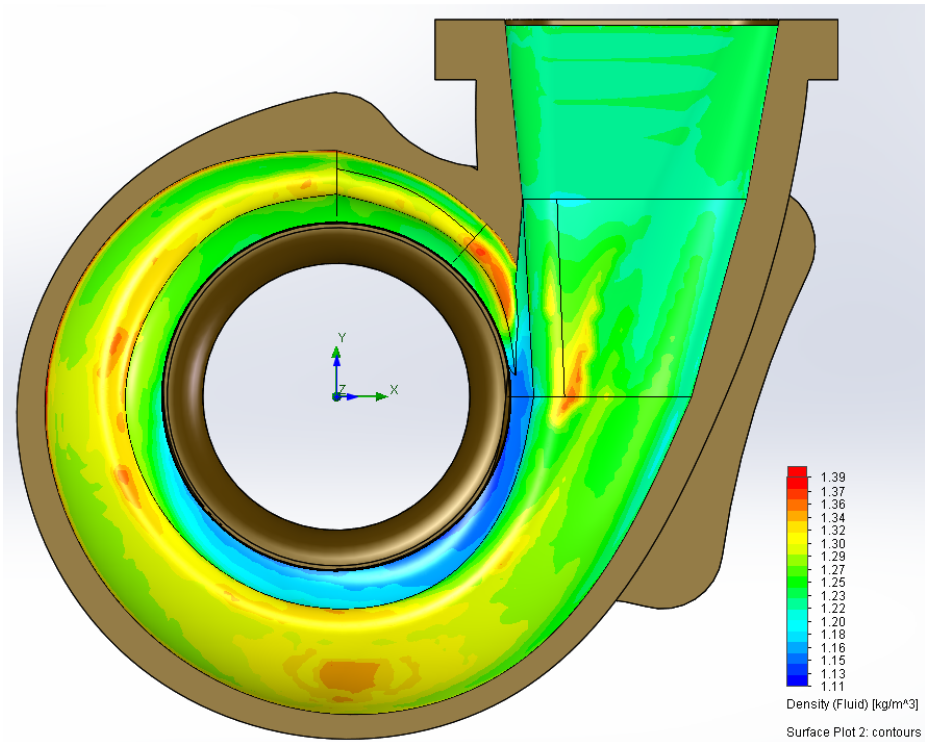


Figure 5.9: Density contour plot

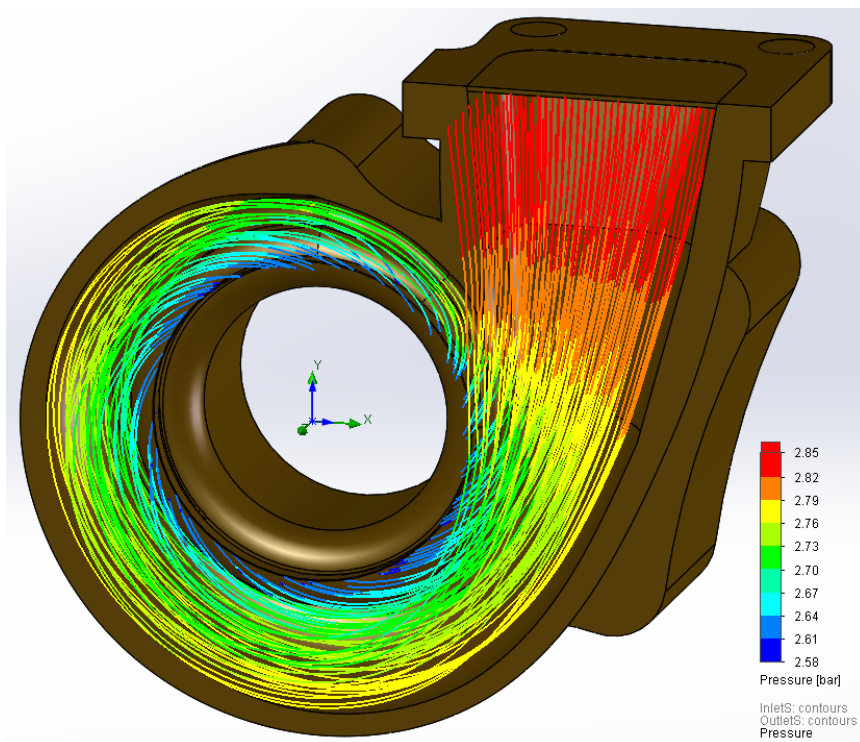


Figure 5.10: Pressure flow trajectories

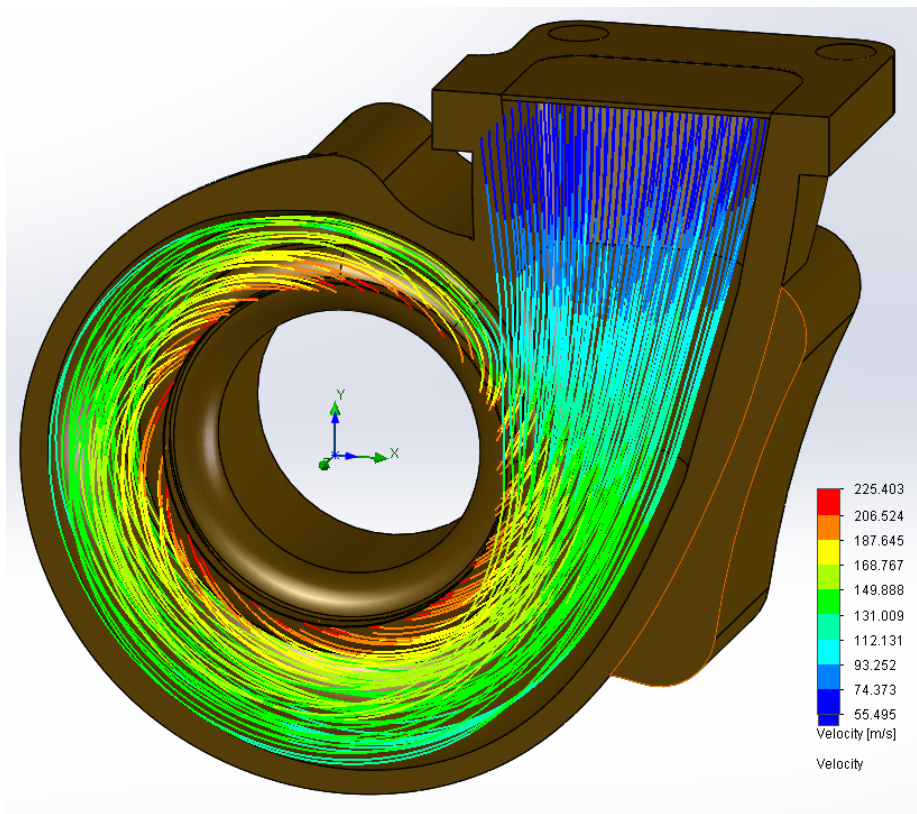


Figure 5.11: Velocity flow trajectories

Chapter 6

GT-Power engine model

The studies have been developed on a 4-cylinder 3.0 litres diesel engine, equipped with a turbocharger. The model is set up to simulate 16 different operating conditions, ranging from a minimum of 850 rpm to a maximum of 3850 rpm.

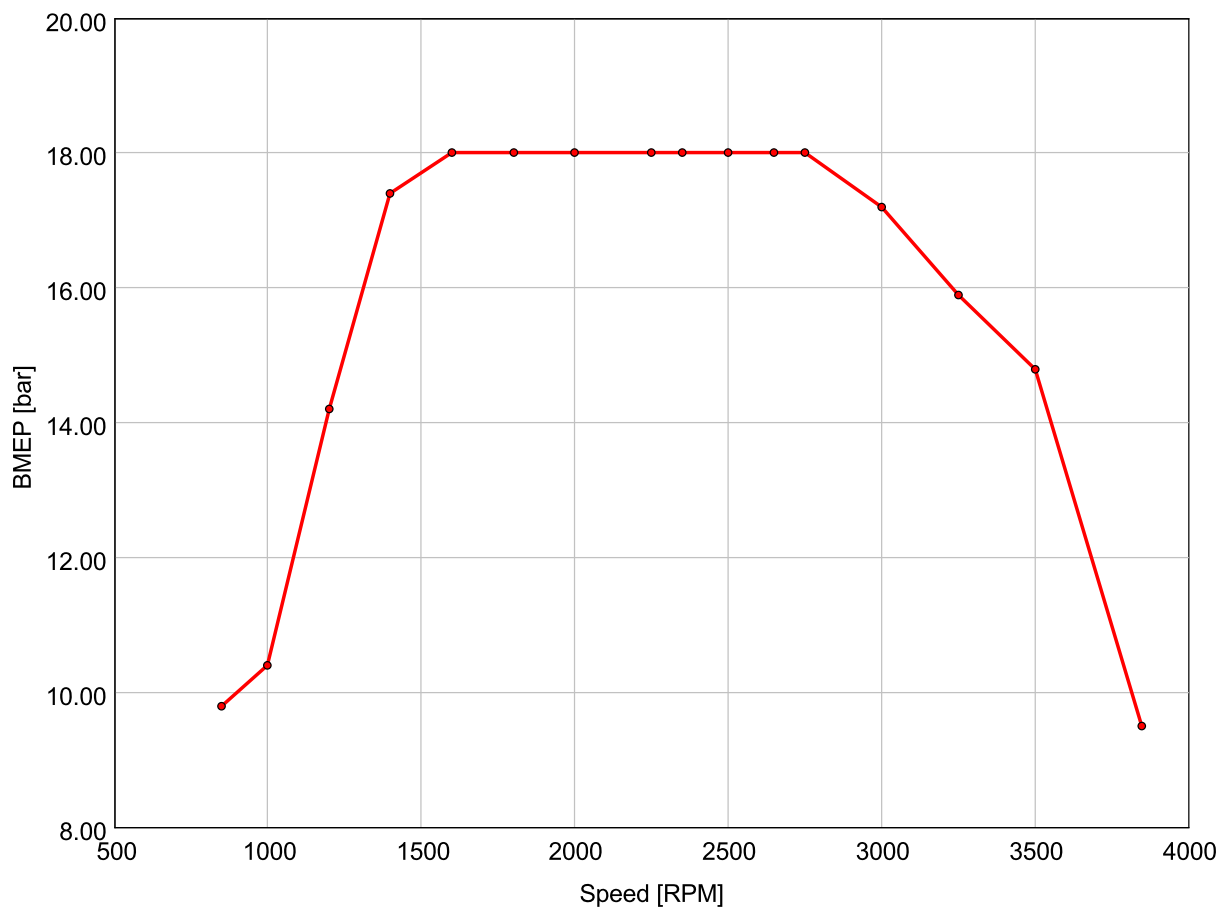


Figure 6.1: Model case setup

Case	#1	#2	#3	#4	#5	#6	#7	#8
rpm	850	1000	1200	1400	1600	1800	2000	2250
bmep	9.80	10.40	14.20	17.40	18.00	18.00	18.00	18.00

Case	#9	#10	#11	#12	#13	#14	#15	#16
rpm	2350	2500	2650	2750	3000	3250	3500	3850
bmep	18.00	18.00	18.00	18.00	17.20	15.90	14.80	9.50

Table 6.1: Case setup working points

6.1 Internal combustion engine

GT-Power allows the creation of a model composed of several interconnected elements in order to simulate each different part of the real engine. In the figure below an overview of the main parts used to build the model is visible.

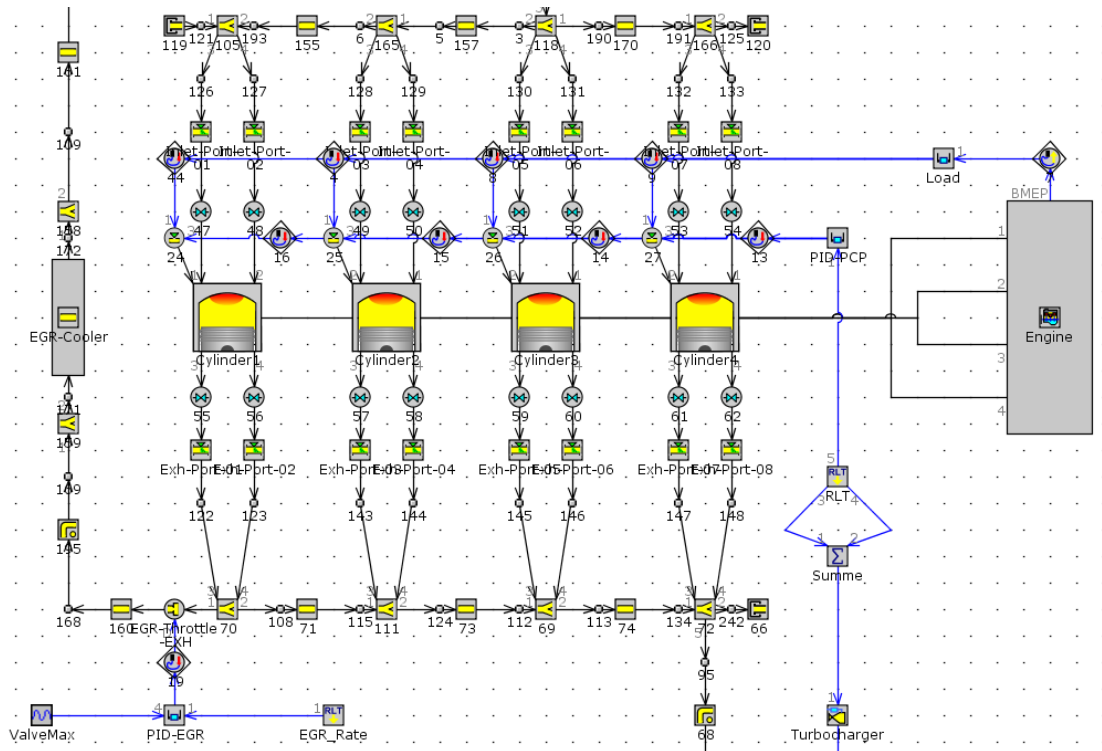


Figure 6.2: GT-Power engine model

The model can be divided into different areas according to the type of process they will simulate:

- combustion process, thermal and fluid-dynamic simulation is associated with the 4 cylinders, injectors, intake and exhaust valves and manifolds as well as EGR system, visible in the middle and left-hand side of the picture;
- mechanics and dynamics of the engine is processed by the *Engine CrankTrain* element visible on the right-hand side.

In addition, a series of PID controllers are required to achieve convergence towards the desired solution: starting from first attempt value (read from case setup), these act in closed loop modifying the process parameters adapting to the needs of the system. The main one is the *Load PID* which imposes the amount of injected fuel, comparing the effective pressure calculated during the previous cycle with the goal to be achieved.

6.2 Turbocharger

The turbocharger unit is connected both to the engine intake and exhaust ports through a series of pipes, and its behaviour is managed by a PID controller. GT-Power allows to simulate the component using 3 items: a compressor, a variable geometry turbine (VGT) and a shaft to connect both elements together, as shown in the figure below.

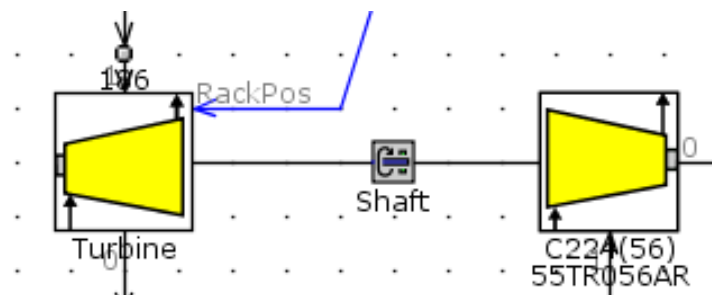


Figure 6.3: GT-Power turbocharger model

Simulations performed in the previous sections regarding 3D CFD have been carried out on a fixed distributor turbine stage, since the main purpose was to analyze the characteristics of the volute and highlight any geometric problems. Here a VGT is adopted to increase performance and better suit engine's requirements.

Because of that, multiple turbine performance maps are required to the solver, one for each different rack position. In that specific case 6 maps were provided which are not enough to properly solve the system. The software in fact interpolates given values to get a full view of turbine performance along all rack position range. Then using a PID controller the value is continuously varied to achieve the target boost pressure. If the pressure results higher than the target, the PID opens the rack increasing turbine's permeability and reducing the boost; likewise, if the pressure delivered by the compressor is lower, the rack is closed increasing turbine inlet pressure and generating more power.

6.3 Standard turbine simulation

Initial tests were performed using the standard turbine, as well as simulated on SolidWorks by 3D CFD, to analyze and evaluate the response and performance of the engine. In order to do that, case setup was populated with data from Table 6.1 and other values relevant for the simulation. Results are summarized in Table 6.2.

<i>Case</i>	<i>RPM</i>	<i>Power [kW]</i>	<i>Rack position</i>	<i>BSFC [g/kWh]</i>	<i>Efficiency</i>
#1	850	20.8	0.428	233.73	0.356
#2	1000	26.0	0.417	225.60	0.369
#3	1200	42.6	0.363	217.35	0.383
#4	1400	60.9	0.359	211.25	0.394
#5	1600	72.0	0.335	210.88	0.395
#6	1800	81.0	0.401	205.80	0.404
#7	2000	90.0	0.403	205.19	0.406
#8	2250	101.2	0.412	205.56	0.405
#9	2350	105.7	0.430	206.56	0.403
#10	2500	112.4	0.462	208.19	0.400
#11	2650	119.2	0.506	209.98	0.396
#12	2750	123.7	0.533	211.71	0.393
#13	3000	128.9	0.561	215.20	0.387
#14	3250	129.1	0.581	219.87	0.379
#15	3500	129.4	0.589	224.57	0.371
#16	3850	91.4	0.633	238.90	0.348

Table 6.2: Standard turbine simulation results

Where *BSFC* represents the *Brake Specific Fuel Consumption* which is obtained, along with efficiency using the following relations:

$$BSFC = \frac{\dot{m}_b}{P_u} \quad (6.1)$$

$$\eta = \frac{1}{BSFC \cdot H_i} \quad (6.2)$$

where \dot{m}_b is the mass flow rate of injected fuel and H_i is the lower heating value of the fuel equal to 43.3 MJ/kg .

In the figure below is shown BSFC trend against speeds through all cases. It will be useful for better data visualization and further comparisons.

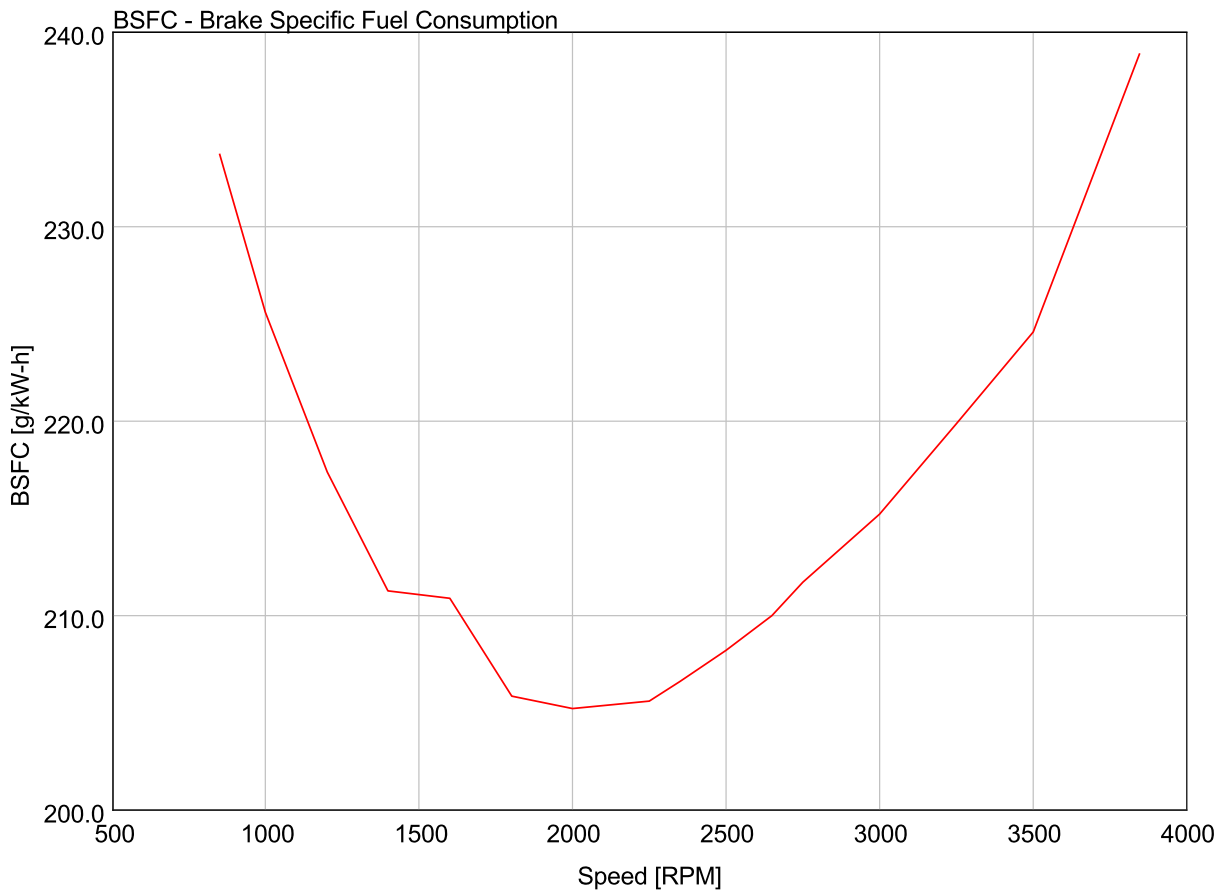


Figure 6.4: Standard turbine BSFC trend

Chapter 7

Turbine size impact on BSFC

Nowadays manufacturers, due to the increasingly stringent regulations regarding pollutant emissions and fuel consumption, are pushing engine's downsizing more and more, to obtain superior performance and reduced consumption. In this compound, turbomatching process it's a significant event and it needs proper care. After results shown in the previous chapter, here changes in the turbine's stage will be taken into account, in order to evaluate the impact they can have on engine performance, in terms of consumption and efficiency.

Two different methodologies are proposed below to evaluate the effect of turbine size variation and at the end results will be compared.

7.1 Mass multiplier scaling method

GT-Power simulates both turbine and compressor elements using performance maps obtained experimentally as results of stationary tests on the real components. As discussed above, for this specific model 6 efficiency maps are available, each of them obtained for different turbine's rack position.

The software allows to define a single turbine element inside the model and assign to it all the maps, which are set through specific windows, as shown in Figure 7.1. To set maps some parameters are required such as: speed, pressure ratio, mass flow and efficiency. In this case data are provided according to the turbine rotational speeds. During pre-calculation routine the software will create interpolating maps for the data provided in order to cover all possible scenarios. For further control and to avoid gross errors, feedback maps are generated to establish the goodness of the approximation achieved by the software.

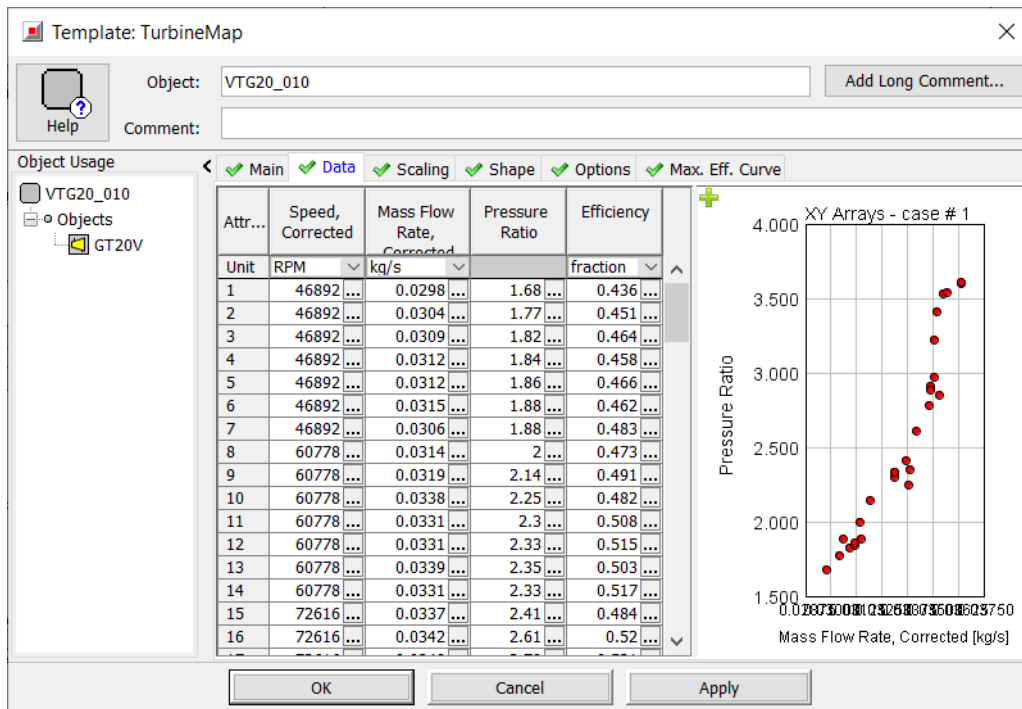


Figure 7.1: Map creation window - GT-Power

Then it is possible to quickly modify the maps using correction factors proposed by the program. Of particular interest for the purpose of this analysis is the *mass multiplier*: the code estimates the instantaneous speed and pressure ratio and using the map gets the mass flow rate; then eventually the rate is multiplied by this factor before it is imposed. In this way, the map has not been actually modified, only the mass flow rate computed by the software was properly modified using the correction factor in order to simulate a different working condition.

Turbine scaling was made considering as a geometric parameter, the A/R ratio already discussed at the paragraph 3.1.2. The correction factor to be implemented in the calculation has therefore been obtained by reading a point on the performance map provided by the manufacturer with a specific A/R ratio and moving that point to a curve with a reduced ratio. Therefore the mass multiplier factor was chosen making appropriate proportion between obtained values of mass flow rate.

Selected value for this first scaling simulation is equal to: $mm = 0.824$, thus a reduction of approximately 17.6%.

Better results in terms of BSFC are obtained at lowest speed with a reduction of almost 2% compared to the standard turbine. However the reduced size of turbine resulting in higher backpressure at the inlet, causes an increase of BSFC at higher loads, as shown in Figure 7.2.

Case	RPM	Power [kW]	Rack position	BSFC [g/kWh]	Efficiency
#1	850	20.8	0.449	234.29	0.355
#2	1000	26.0	0.458	226.26	0.368
#3	1200	42.6	0.451	217.10	0.383
#4	1400	60.9	0.471	210.59	0.395
#5	1600	72.0	0.485	208.11	0.400
#6	1800	81.0	0.493	207.03	0.402
#7	2000	90.0	0.494	206.71	0.403
#8	2250	101.2	0.513	207.15	0.402
#9	2350	105.7	0.538	208.29	0.400
#10	2500	112.4	0.571	210.07	0.396
#11	2650	119.2	0.609	212.71	0.391
#12	2750	123.7	0.630	215.16	0.387
#13	3000	128.9	0.652	219.71	0.379
#14	3250	129.1	0.670	225.23	0.370
#15	3500	129.4	0.678	230.52	0.361
#16	3850	91.4	0.720	245.20	0.339

Table 7.1: Scaled turbine simulation results, mm = 0.824

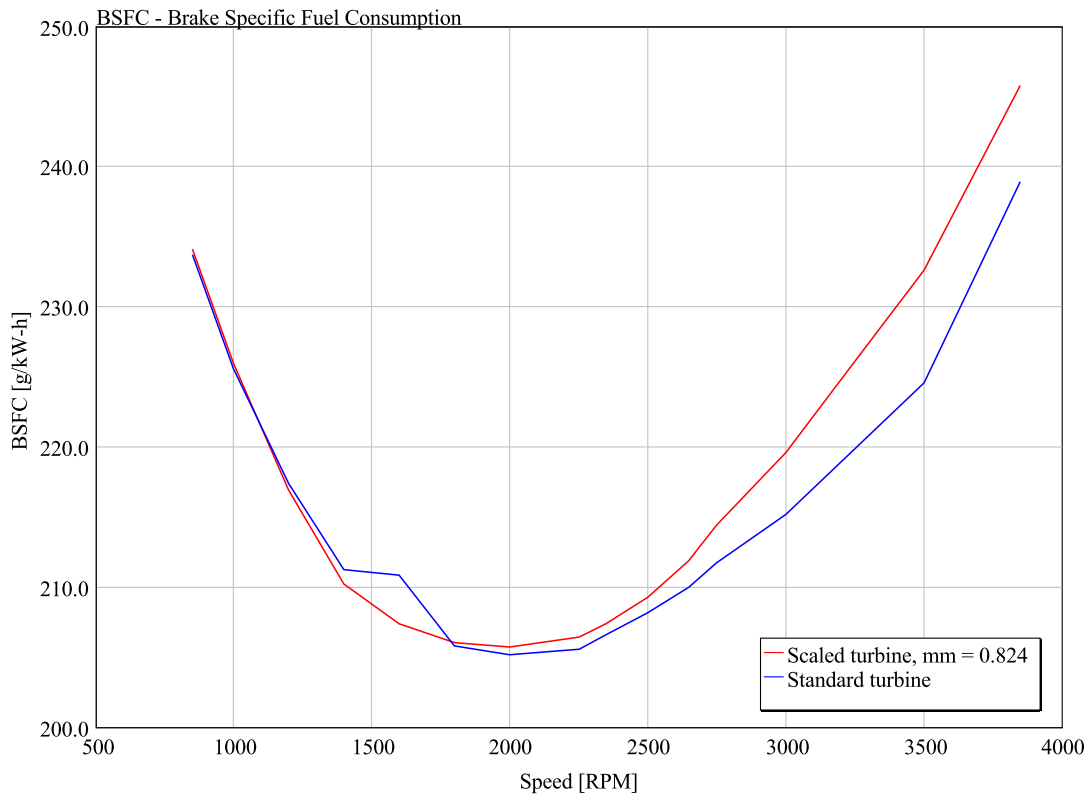


Figure 7.2: BSFC trend comparison, mm = 0.824

7.2 Fluid-dynamic similitude scaling method

Before proceeding with further simulations it is worth asking whether the method described above can give reliable results. Actually, some considerations deserve to be made about it since it does not take into account variation in the corrected speed of the turbine rotor, but it just scales the mass flow rate.

It is clear that if accurate analysis are required, experimental tests should be performed on the new turbines in order to get reliable maps. Anyways, since this approach is not always applicable, convenient methods were developed through the years to speed up the process in a predictable way. In this section it is going to be presented a different procedure derived from the approach of fluid-dynamic similitude [12].

Both turbine and compressor performance maps depend on working fluid and some design parameters such as trim (see 3.1.1), diameter and the A/R ratio (see 3.1.2) associated with the housing design. As long as these parameters are known it is possible to obtain adimensional coefficient of mass flow rate ϕ and Mach number based on the rotor tip speed c_0 :

$$\phi = \dot{m}_{corr} \frac{\sqrt{R}}{D^2} \quad (7.1)$$

$$c_0 = \left(\frac{2\pi}{60}\right) N_{corr} \frac{D}{\sqrt{\gamma R}} \quad (7.2)$$

where respectively, \dot{m}_{corr} is the corrected mass flow rate defined as $\dot{m}_{corr} = \frac{\dot{m}\sqrt{T}}{p}$ and N_{corr} is the corrected speed which equals to $N_{corr} = \frac{N}{\sqrt{T}}$. By imposing this values to be constant for both standard and scaled turbine, it is possible to obtain the new corrected mass flow rate and speed as follows:

$$\dot{m}'_{corr} = \frac{\dot{m}_{corr} D'^2}{D^2} \quad (7.3)$$

$$N'_{corr} = \frac{N_{corr} D'^2}{D^2} \quad (7.4)$$

Using this procedure new turbine maps have been evaluated. To make consistent comparison with the *mass multiplier* scaling method, a reduction of approximately 17% on the rotor diameter has been chosen. All the available maps, have been modified and integrated in

GT-Power through the window shown in Figure 7.1, some examples are shown below.

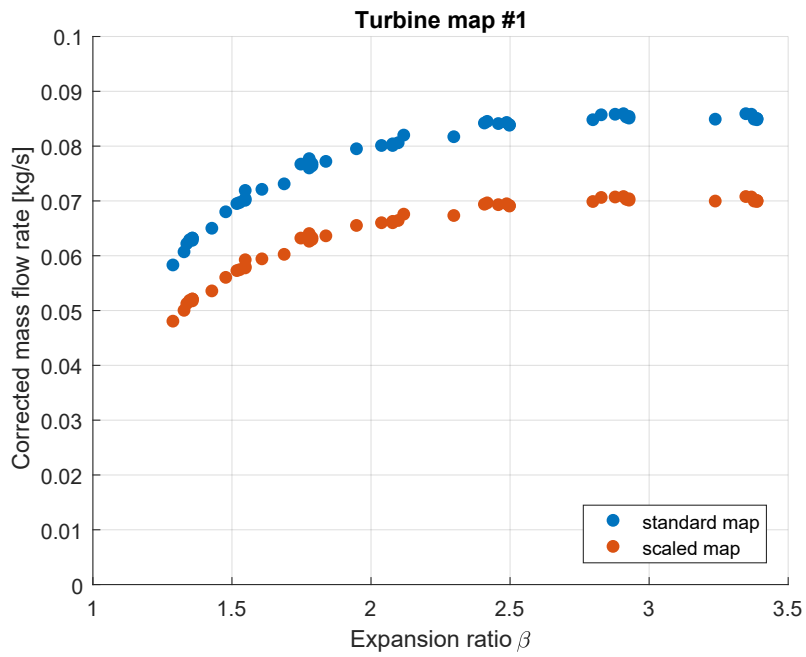


Figure 7.3: Fluid-dynamic scaled turbine map - 1

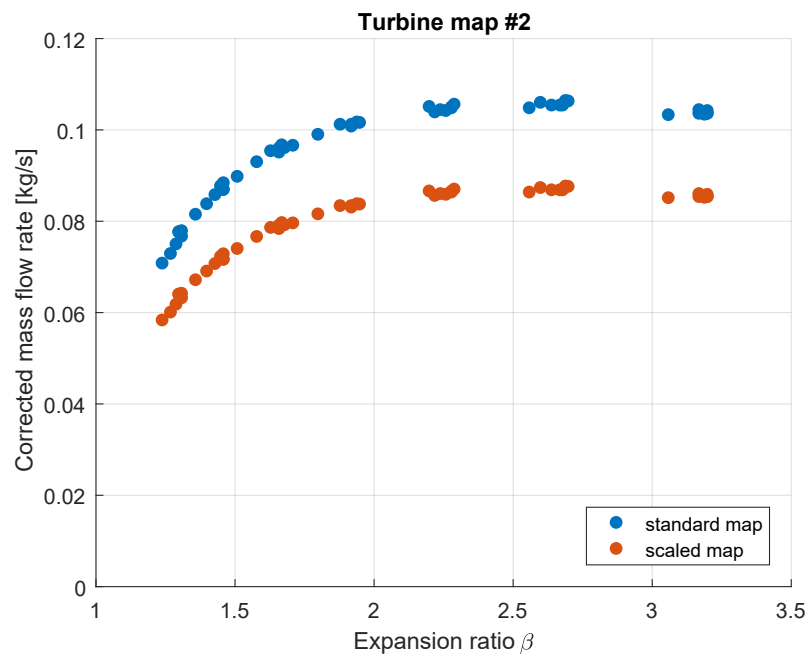


Figure 7.4: Fluid-dynamic scaled turbine map - 2

Results obtained using new maps are collected in the following table.

<i>Case</i>	<i>RPM</i>	<i>Power [kW]</i>	<i>Rack position</i>	<i>BSFC [g/kWh]</i>	<i>Efficiency</i>
#1	850	20.8	0.449	234.29	0.355
#2	1000	26.0	0.458	226.26	0.368
#3	1200	42.6	0.451	217.10	0.383
#4	1400	60.9	0.471	210.59	0.395
#5	1600	72.0	0.485	208.11	0.400
#6	1800	81.0	0.493	207.03	0.402
#7	2000	90.0	0.494	206.70	0.403
#8	2250	101.2	0.513	207.15	0.402
#9	2350	105.7	0.538	208.29	0.400
#10	2500	112.4	0.571	210.07	0.396
#11	2650	119.2	0.609	212.71	0.391
#12	2750	123.7	0.630	215.16	0.387
#13	3000	128.9	0.652	219.71	0.379
#14	3250	129.1	0.670	225.27	0.370
#15	3500	129.4	0.678	230.52	0.361
#16	3850	91.4	0.721	245.04	0.340

Table 7.2: Scaled turbine simulation results, FDS

7.2.1 Consideration about methods usage

Comparing results obtained from the two proceeding ways, in this specific case, it can be pointed out that no substantial differences subsist which can lead to prefer one of the two methods with respect to the other. Both the BSFC, the rack position, inlet and outler pressure, as well as the efficiency of the system show very slight difference. Therefore, since modifying and updating the different maps within the software could result in a time consuming process, the *mass multiplier* method will be used for further speculations over this topic.

7.3 Further turbine simulations

In addition to previous simulations, here are reported other studies performed on the turbine for completeness and greater overview of results, using the mass multiplier method.

7.3.1 Turbine size x0.9

Results obtained using a correction factor of $mm = 0.908$.

Case	RPM	Power [kW]	Rack position	BSFC [g/kWh]	Efficiency
#1	850	20.8	0.461	233.88	0.356
#2	1000	26.0	0.453	225.81	0.369
#3	1200	42.6	0.417	216.72	0.384
#4	1400	60.9	0.418	210.44	0.396
#5	1600	72.0	0.443	207.52	0.401
#6	1800	81.0	0.454	206.26	0.404
#7	2000	90.0	0.457	205.69	0.405
#8	2250	101.2	0.468	206.12	0.404
#9	2350	105.7	0.491	207.04	0.402
#10	2500	112.4	0.527	208.74	0.399
#11	2650	119.2	0.573	210.62	0.395
#12	2750	123.7	0.601	212.43	0.392
#13	3000	128.9	0.624	216.46	0.385
#14	3250	129.1	0.641	221.58	0.376
#15	3500	129.4	0.648	226.55	0.367
#16	3850	91.4	0.693	240.85	0.346

Table 7.3: Scaled turbine simulation results, mm = 0.908

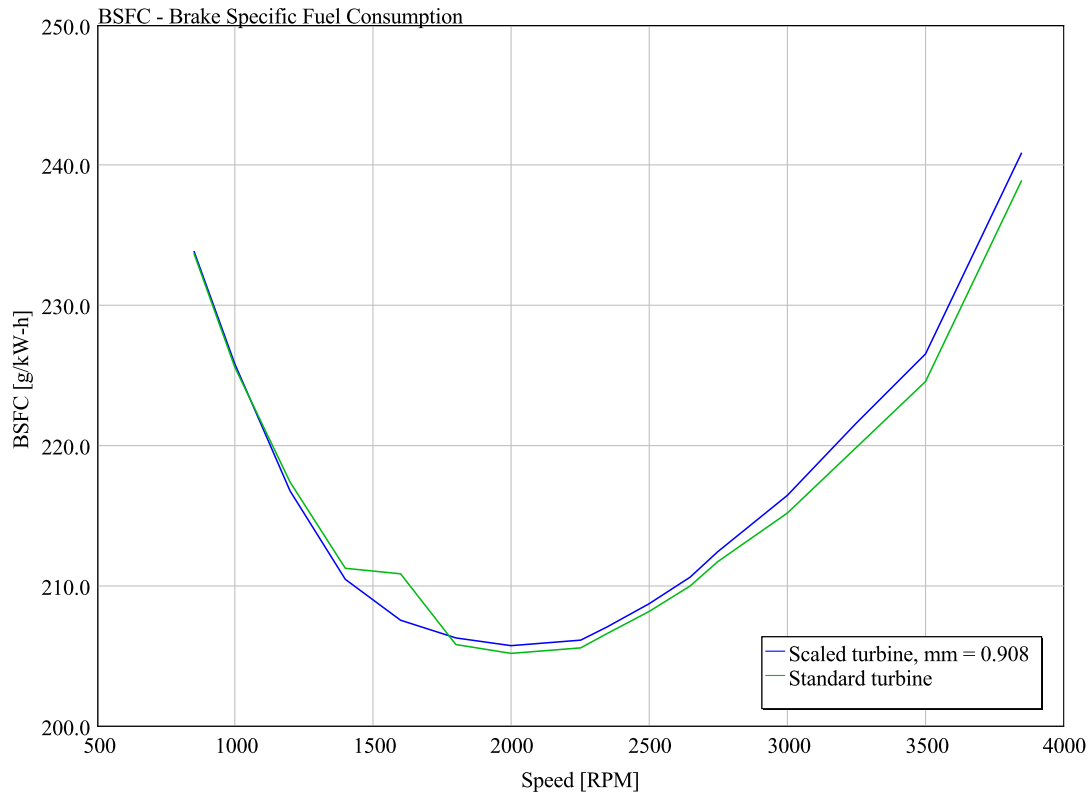


Figure 7.5: BSFC trend comparison, mm = 0.908

This configuration shows a clear improvement over the previous case: at low revs the curves are basically overlapping, with a more marked consumption improvement in the 1400-1800 rpm range. At higher regimes, consumption increases compared to the standard turbine, also in this case due to the increasing exhaust backpressure, which deteriorates the pumping cycle and thus losses for fluid replacement.

7.3.2 Turbine size x1.1

Hereafter the results obtained by simulating a larger turbine are proposed ($mm = 1.100$).

<i>Case</i>	<i>RPM</i>	<i>Power [kW]</i>	<i>Rack position</i>	<i>BSFC [g/kWh]</i>	<i>Efficiency</i>
#1	850	20.8	0.393	233.66	0.356
#2	1000	26.0	0.375	225.75	0.369
#3	1200	42.6	0.304	218.02	0.382
#4	1400	60.9	0.300	212.52	0.392
#5	1600	72.0	0.285	212.36	0.392
#6	1800	81.0	0.290	211.28	0.394
#7	2000	90.0	0.294	211.01	0.394
#8	2250	101.2	0.325	210.13	0.396
#9	2350	105.7	0.356	209.05	0.398
#10	2500	112.4	0.402	207.75	0.401
#11	2650	119.2	0.443	209.54	0.397
#12	2750	123.7	0.467	211.21	0.394
#13	3000	128.9	0.494	214.62	0.388
#14	3250	129.1	0.512	219.25	0.380
#15	3500	129.4	0.519	223.94	0.372
#16	3850	91.4	0.571	237.65	0.350

Table 7.4: Scaled turbine simulation results, $mm = 1.100$

Simulating a larger turbine, gives unsatisfactory results since, despite slight improvements gained at higher operation regimes, at low-middle loads the situation has worsened considerably, with an efficiency reduction of almost 3% as shown in Figure 7.6.

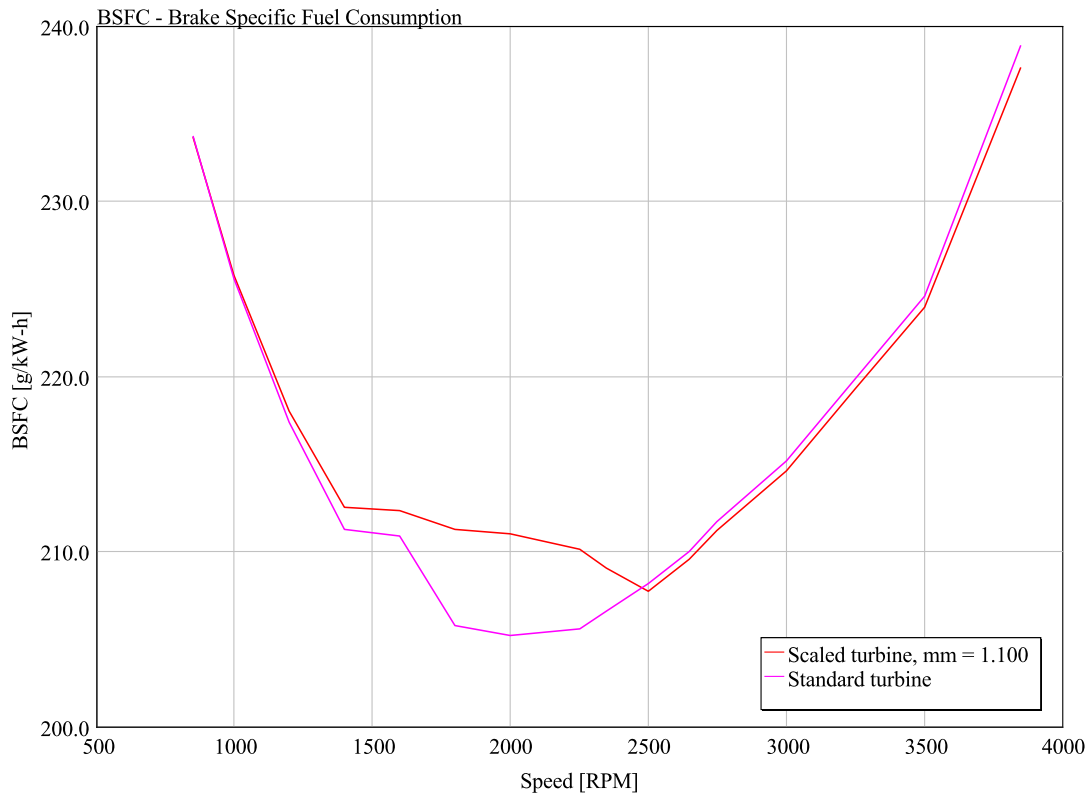


Figure 7.6: BSFC trend comparison, mm = 1.100

7.4 Results comparison

The data obtained by simulating different turbine sizes show very different outcomes in terms of engine performance and in particular fuel consumption.

The adoption of a smaller turbine allows to obtain advantages mainly in the area of medium loads, with improvements in consumption up to almost 2%; on the other hand, the reduced dimensions of the turbine housing cause greater backpressure which leads to a worsening of the pumping cycle with a consequent loss of performance and an increase in consumption.

The situation improves by slightly increasing the size of the turbine, referring to the case in which $mm = 0.908$ was used. Taking a look at Figure 7.8, at low loads the situation remains almost unchanged, both compared to the previous case and the standard one: the consumption curve is softer and improvements are achieved starting from 1200 up to 1800 rpm. Similarly to the previous case, the smaller size of the turbine housing worsens the efficiency at high loads due to the higher backpressure, but in this case the deterioration is much lower and can be considered acceptable, taking into account variance on the available data and on the simulations themselves.

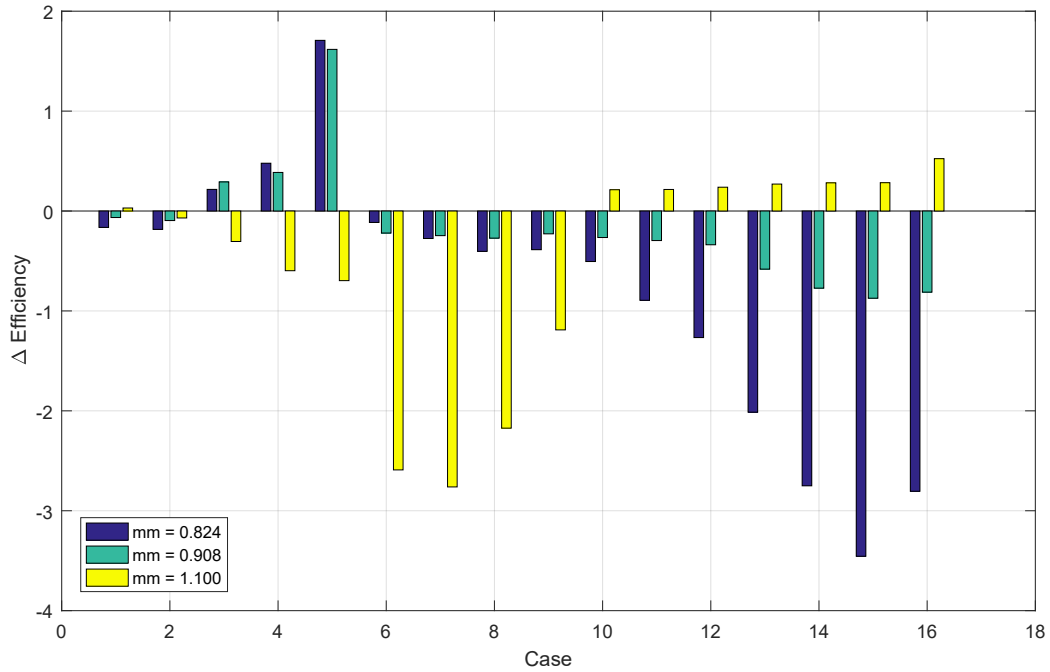


Figure 7.7: Efficiency runouts compared to basic turbine

mm	#1	#2	#3	#4	#5	#6	#7	#8
0.824	-0.16	-0.18	0.22	0.48	1.71	-0.11	-0.28	-0.40
0.908	-0.07	-0.10	0.29	0.39	1.62	-0.22	-0.25	-0.27
1.100	0.03	-0.07	-0.30	-0.60	-0.70	-2.59	-2.76	-2.17

mm	#9	#10	#11	#12	#13	#14	#15	#16
0.824	-0.39	-0.51	-0.89	-1.27	-2.01	-2.75	-3.46	-2.80
0.908	-0.23	-0.27	-0.30	-0.34	-0.58	-0.77	-0.87	-0.81
1.100	-1.19	0.21	0.22	0.24	0.27	0.28	0.28	0.52

Table 7.5: Efficiency runouts - percentage values

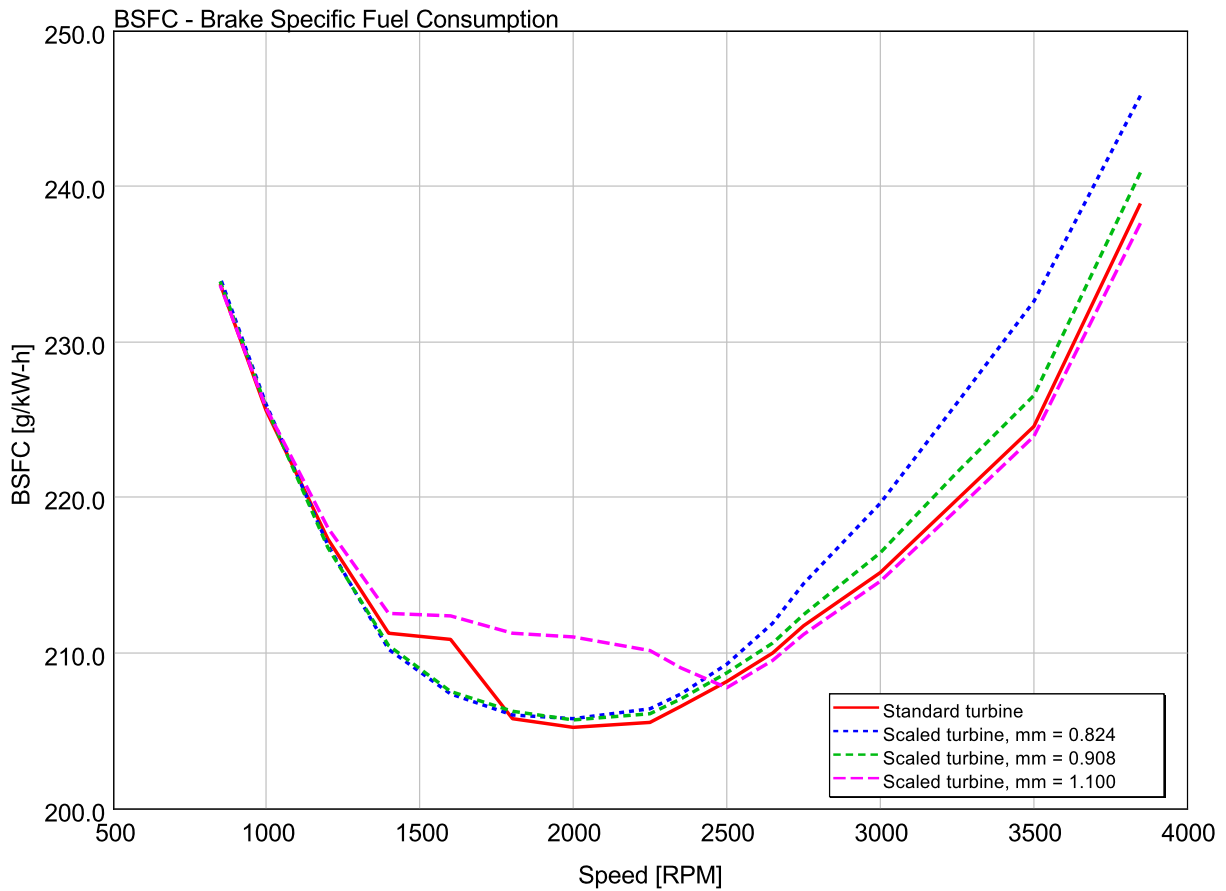


Figure 7.8: BSFC trends comparison

As could be hypothesized, the scenario is reversed if a turbine larger than the standard one is considered. Even in this application, as in all contexts, it's not possible to get a solution that can meet all expectations and a compromise that fits all requirements must be found.

For this reason, analyzing the picture in Figure 7.8 it can be concluded that despite slight worsening at high loads, the substantial improvement obtained in the area of medium loads tipped the balance towards a choice that leads to slightly reduce the size of the turbine.

7.5 Medium load deterioration analysis

From previously carried out conclusions, it was found that an increase in the size of the turbine causes a worsening of the overall efficiency of the engine with a significantly increase of BSFC in the area of medium loads. To explain this behavior it is necessary to refer to some operating parameters of the turbine and of the engine work cycle, as follows.

7.5.1 Turbine expansion ratio β

Taking into account the standard and the enlarged turbine (mm = 1.1) and comparing their expansion ratio in the same plot versus the brake specific fuel consumption, a particular trend immediately emerges as in the picture below.

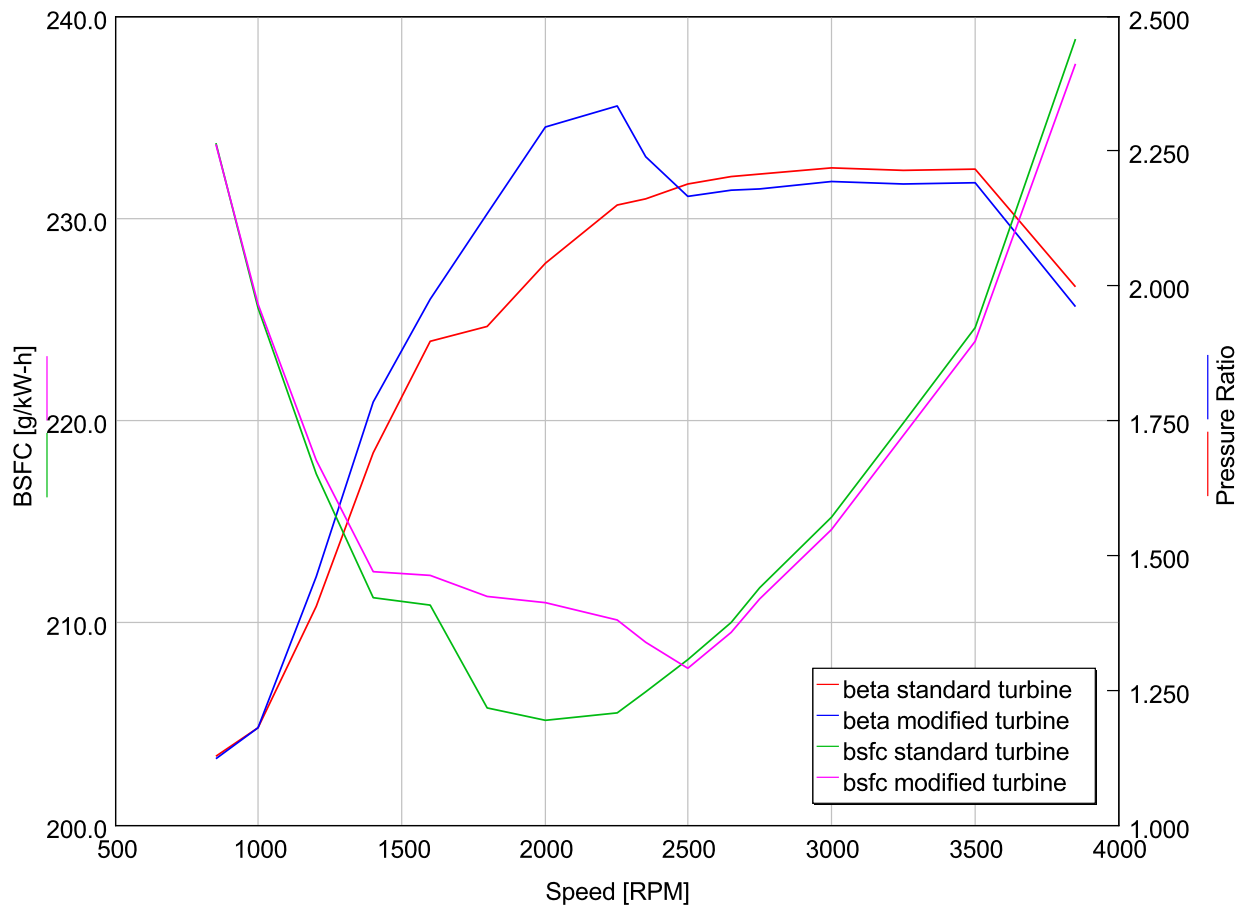


Figure 7.9: Different turbine expansion ratios comparison

The graph clearly shows that in the region where there is a worsening of the engine efficiency, the turbine has a greater expansion ratio than the standard configuration, which presupposes an increase in backpressure with consequent losses during the fluid replacement cycle.

This behavior is probably due to the control strategy of the turbine rack position: in fact this has not been modified and consequently is optimized only for the standard configuration, smaller than the modified one being considered (this explains why reducing the size of the turbine does not affect the efficiency the same way). Therefore, considering to modify this specific control could result in better performance results over all engine operational regimes.

7.5.2 Pumping loop

This hypothesis is confirmed by the trend of the discharge pressures during the fluid replacement cycle for the areas affected by the performance decay, as shown below.

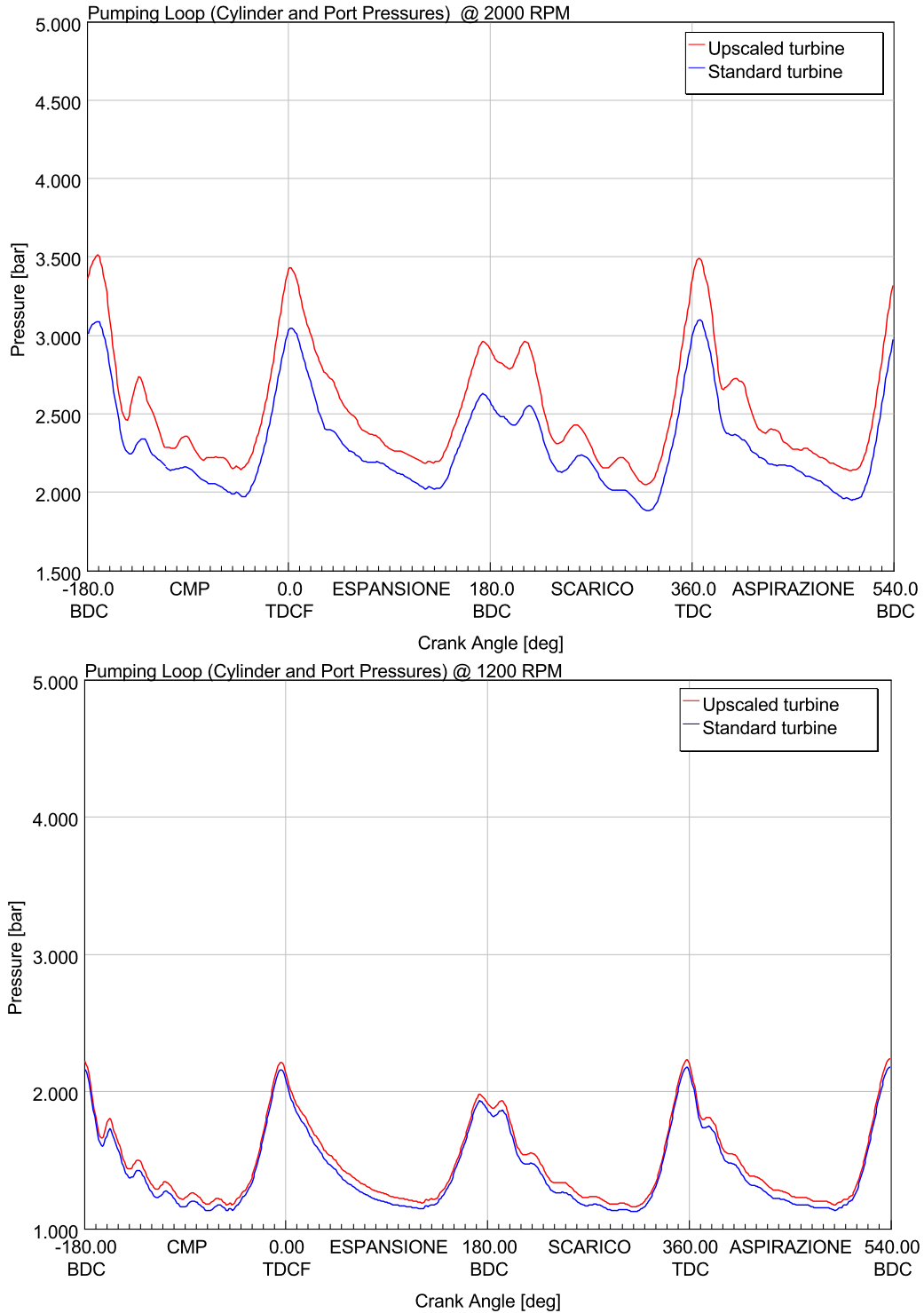


Figure 7.10: Exhaust pressure at different regimes

7.6 Control strategy

The combustion process is very complex and it takes place through a series of steps that lead to the generation of torque. In particular for diesel engines, after the mixture has been injected into the combustion chamber and the ignition delay τ_i has elapsed (which does not scale with the rotational speed of the engine) the premixed combustion phase starts. This translates into a sharp increase of pressure inside the chamber with a peak in terms of heat release rate HRR, consequent fatigue stresses on the engine parts and loud noise typical of these engines. Thanks to new technologies, such as the use of the common rail, which allows to use higher injection pressures (up to 2000 bar), it has been possible to contain and improve some of these parameters but a compromise needs to be found.

In accordance with traditional literature the combustion process should have an appropriate timing in order to extract the maximum potential from the fuel and reach high performance. One of the parameters used to obtain this specific phasing is the *MFB* which stands for Mass Fraction Burned. Best results are obtained for MFB50, meaning the 50% of mass burned, situated around 10° ATDC (After Top Dead Center). An example of pressure and MFB trends are shown in the picture below.

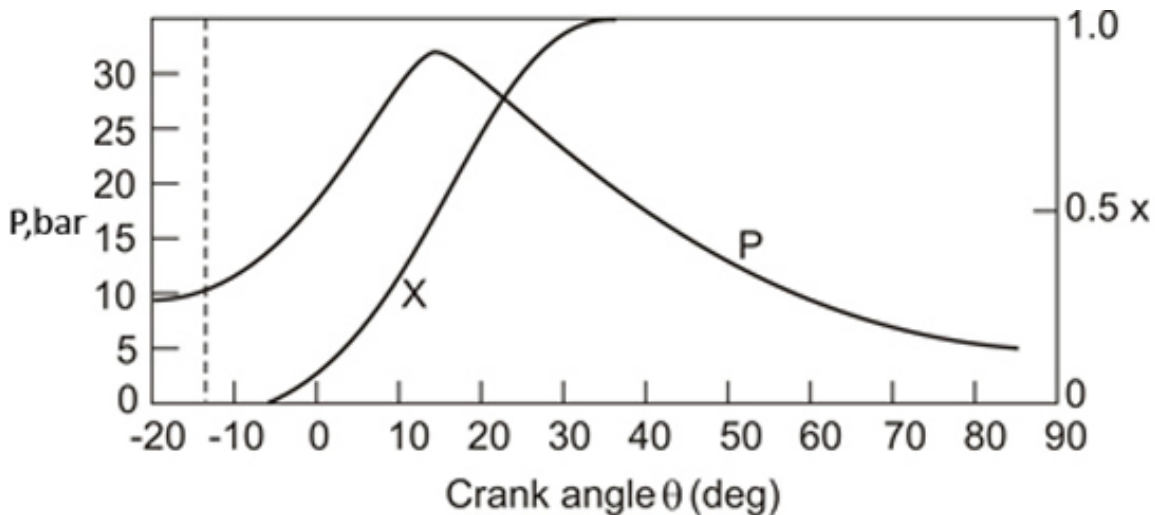


Figure 7.11: Pressure and MFB trends

After injection starts, there's an initial delay and then the mass fraction burned increases with a cubic trend, usually reaching reaching its completion after $40/50^\circ$ ATDC.

Unfortunately this approach is not always applicable to engine's control strategy due to several reasons. In the model object of the calculations shown in the previous chapters, the engine management strategy was based on the control of the maximum pressure reached (BMEP), achieved by using a PID controller to calculate the amount of fuel to be injected cycle by cycle to obtain the expected pressure. A RLT element is used to compare the results from the previous cycle to the actual one and make appropriate adjustments. In figure 7.10 is shown the architecture of the controller.

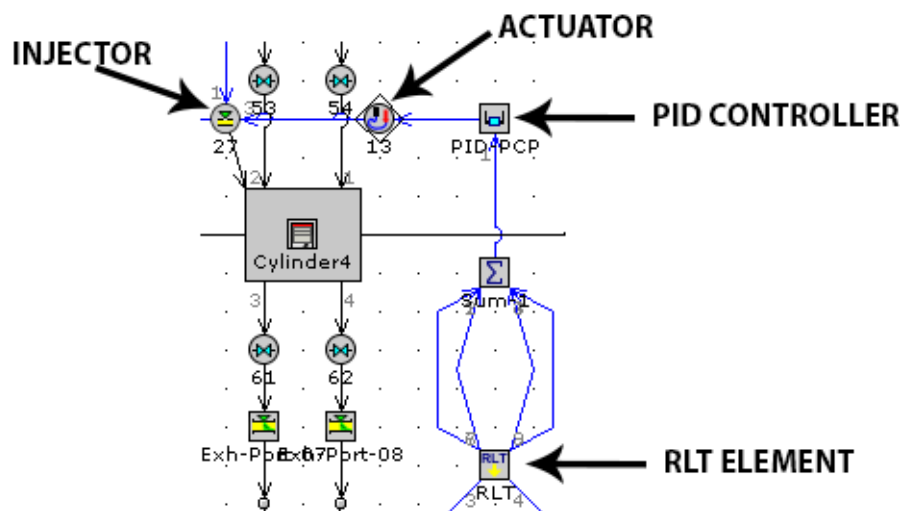


Figure 7.12: PID controller scheme

To achieve the goal of having the combustion MFB50 centered around 10° ATDC and get rigorous results, the 4 reference signals relating to the pressures in the 4 cylinders were taken and sent to an element that gives as output the average value and then sent to the PID that controls the injectors and therefore the quantity of fuel injected into the chamber. A target value along with proportional and integral gain are set within the PID control window.

Target for the Input Signal		10 ...
Gains Specification / Calculation		
Gains Specified		
Proportional Gain		0.05 ...
<input checked="" type="radio"/> Integral Gain		1 ...
Derivative Gain		ign ...
Derivative Time Constant	s	def ...

Figure 7.13: PID setting window

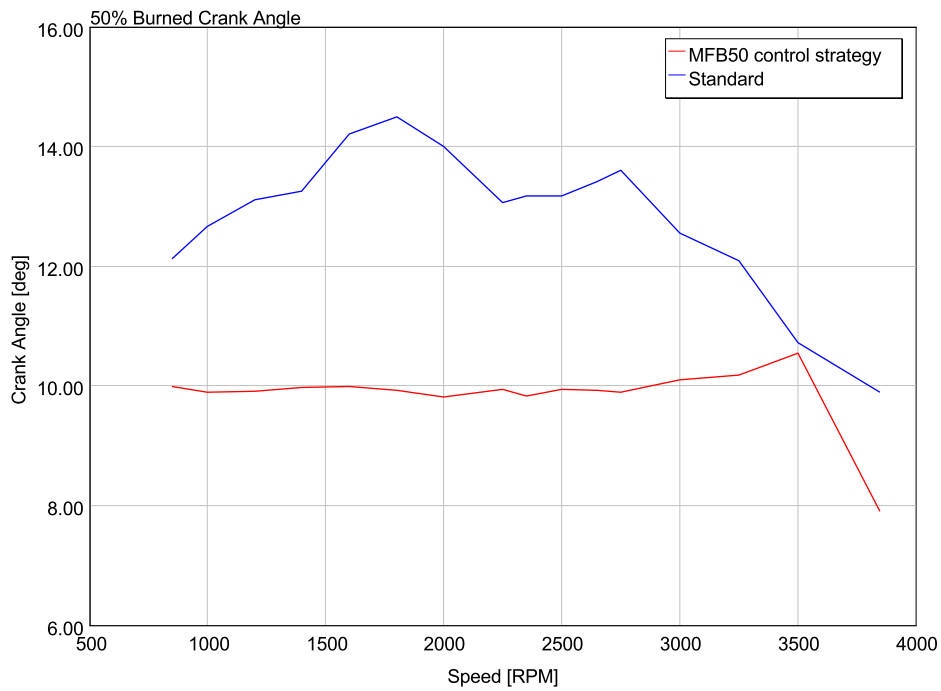


Figure 7.14: MFB50 trend comparison

As shown in picture 7.12 using this strategy is possible to center the combustion process to the desired target in almost all working points with a nice gap, which also results in a significant reduction of the angle at Start of Injection (SOI).

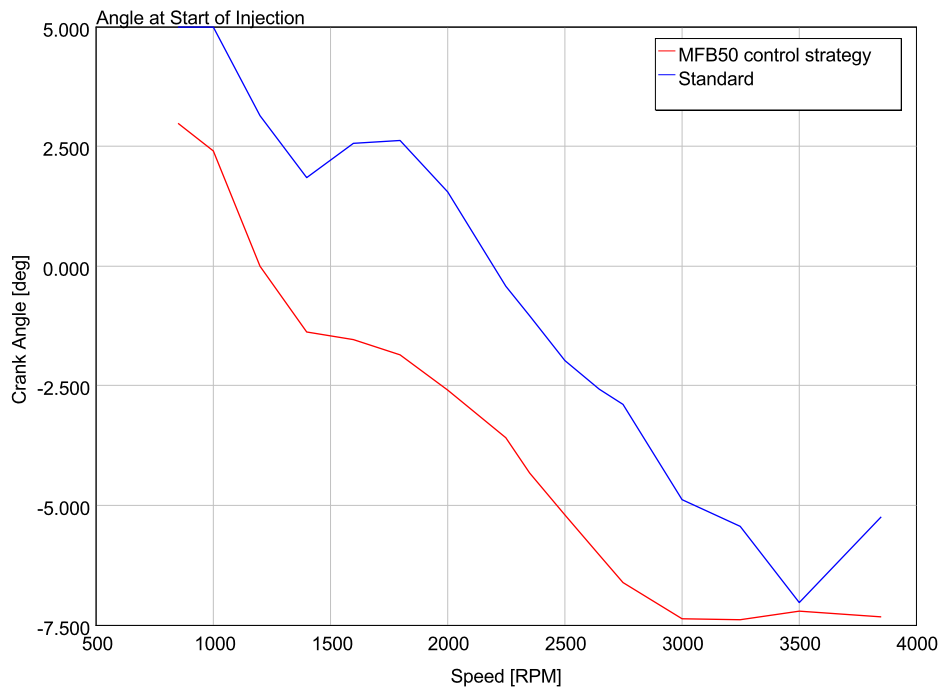


Figure 7.15: SOI angle using MFB50 control strategy

This leads to a slight decrease in the quantity of injected fuel as visible in picture 7.14, maintaining the same performance, since the indicated efficiency increases. In fact, BSFC also decreases, as shown in pictures 7.15.

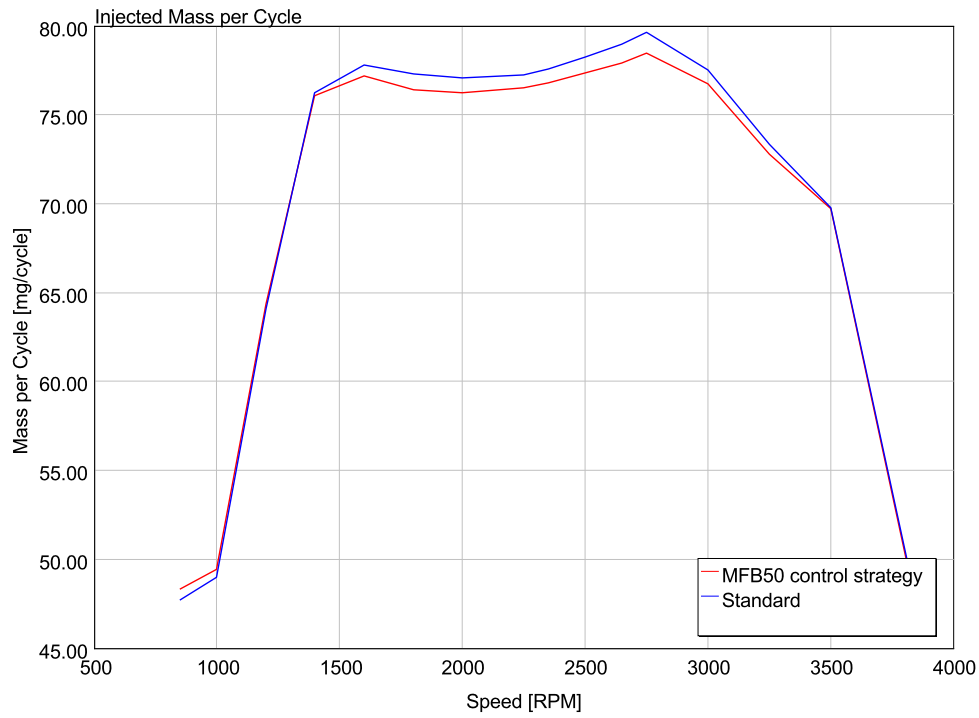


Figure 7.16: Injected mass using MFB50 control strategy

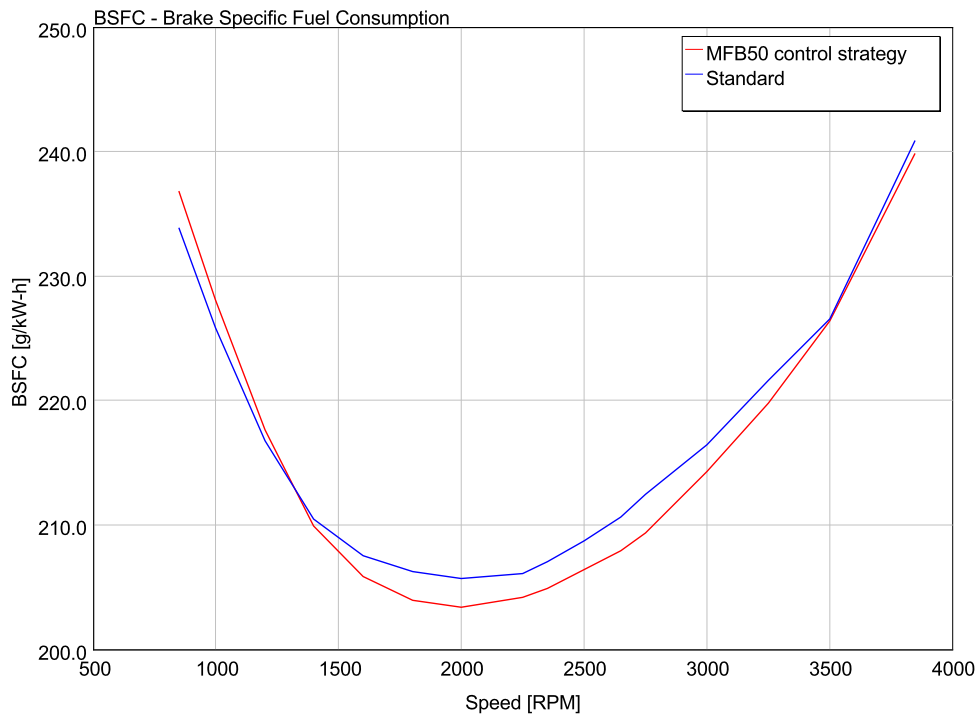


Figure 7.17: BSFC trend using MFB50 control strategy

Furthermore, using this control strategy by modifying the timing of the combustion process, enables to improve the output conditions of the exhaust gases. Analyzing the admission conditions at the turbine, the inlet temperature is lower thanks to the better timing, which allows to reduce thermal stresses fatigue associated problems, such as creep which can cause turbine failure.

7.7 Maximum braking torque

The final task of this paper is to find the maximum torque that can be supplied by the engine. During all the simulations previously described, the working points were simulated by giving to the software as input data in the case setup, different target values such as bmep, boost pressure, speed, etc. Thus, one way to squeeze everything possible out of the engine is to set a very high BMEP target value, which cannot really be obtained due to physical limitations and consequently saturate other components to evaluate which is the maximum power that the engine can deliver.

Setting such high target values caused at first the injector to saturate, since an upper limit was set within the component used for the simulation. Therefore, to estimate the engine real potential, the limit over the maximum injected fuel was removed and new calculations were performed.

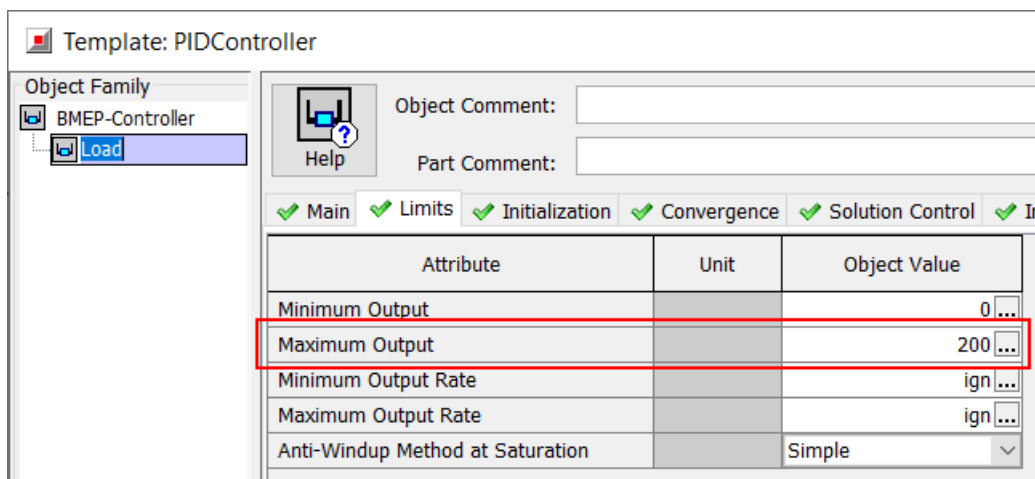


Figure 7.18: Load PID controller setting window

Here the setting tab for the load controller, the maximum output was increased up to 200 to evaluate new performance.

In the figure above, continuous lines show results in terms of power and torque delivered by the engine at its maximum performance, while dotted ones represent the standard engine trends.

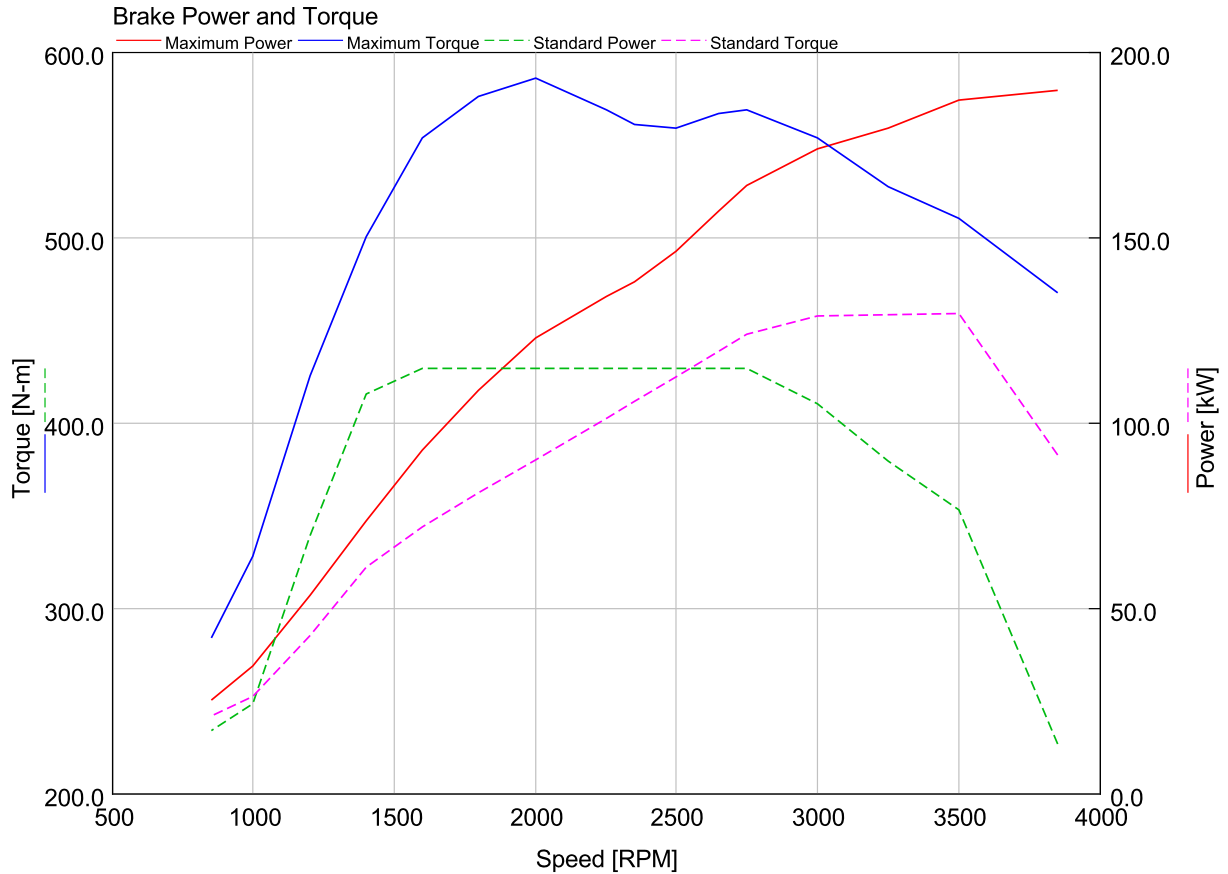


Figure 7.19: Maximum Power and Torque compared to standard engine

Table 7.6 reports numerical data to better identify achieved improvements, with an increase in the supplied power over 46% and a torque raise of more than 36%.

Engine setup	Power [kW]	Torque [Nm]
Standard configuration	129.4	430
Maximum performance	189.6	586
Increment	+ 46.5%	+ 36.3%

Table 7.6: Power and Torque values

For completeness, charts relating to the max BMEP and the maximum pressure reached inside the combustion chamber are shown below.

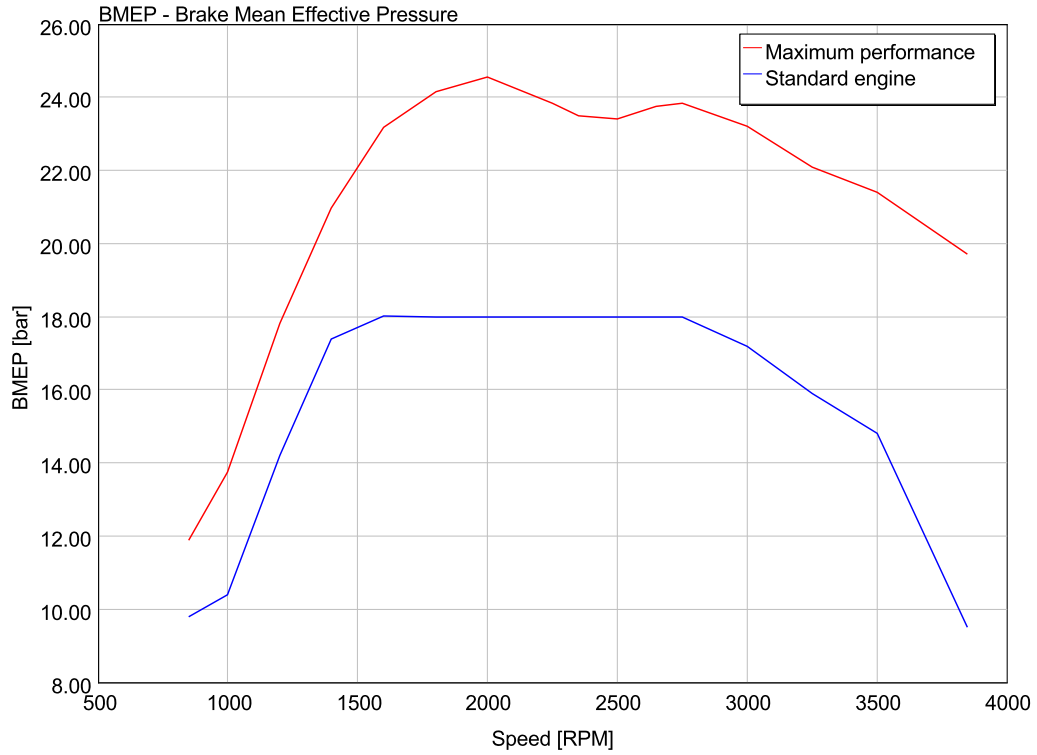


Figure 7.20: BMEP trend for maximum performance and standard engine

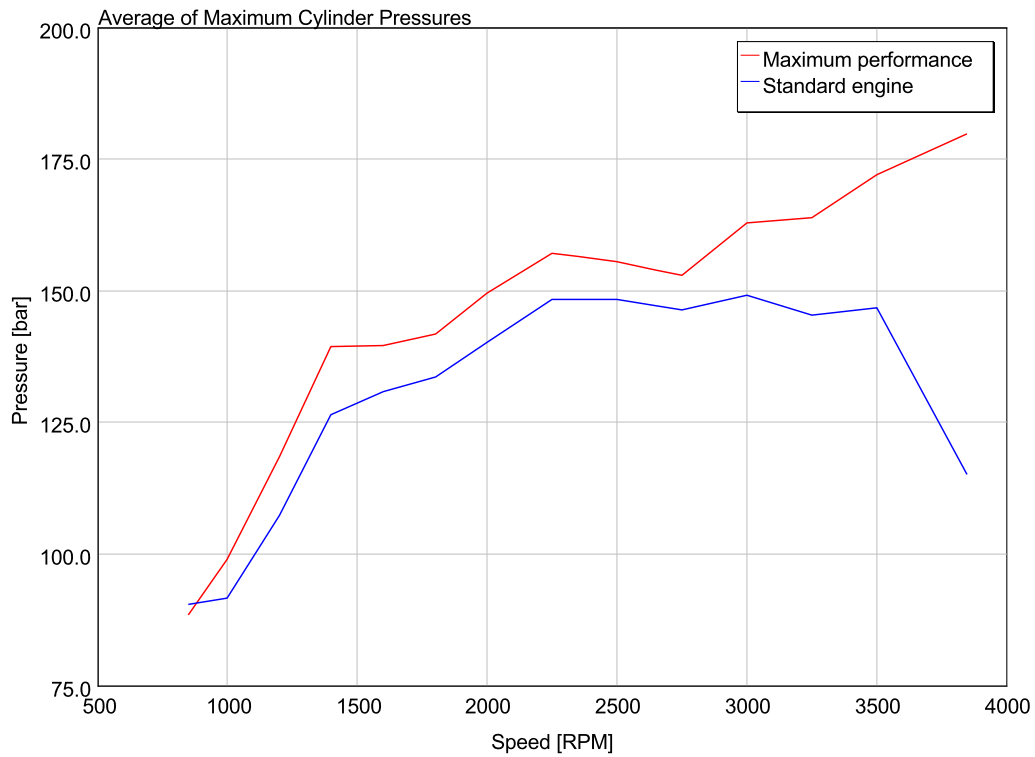


Figure 7.21: Cylinder pressure trend for maximum performance and standard engine

Figure 7.21 clearly shows the maximum pressure inside the cylinder: pressure in the standard engine is safely maintained below 150 bar, while in the maximum performance crosses that threshold which can cause engine damage in the long run. For further detail, the chart of α , Air-to-Fuel ratio is shown: the value saturates at 15, for reasons relating to the smoke limit.

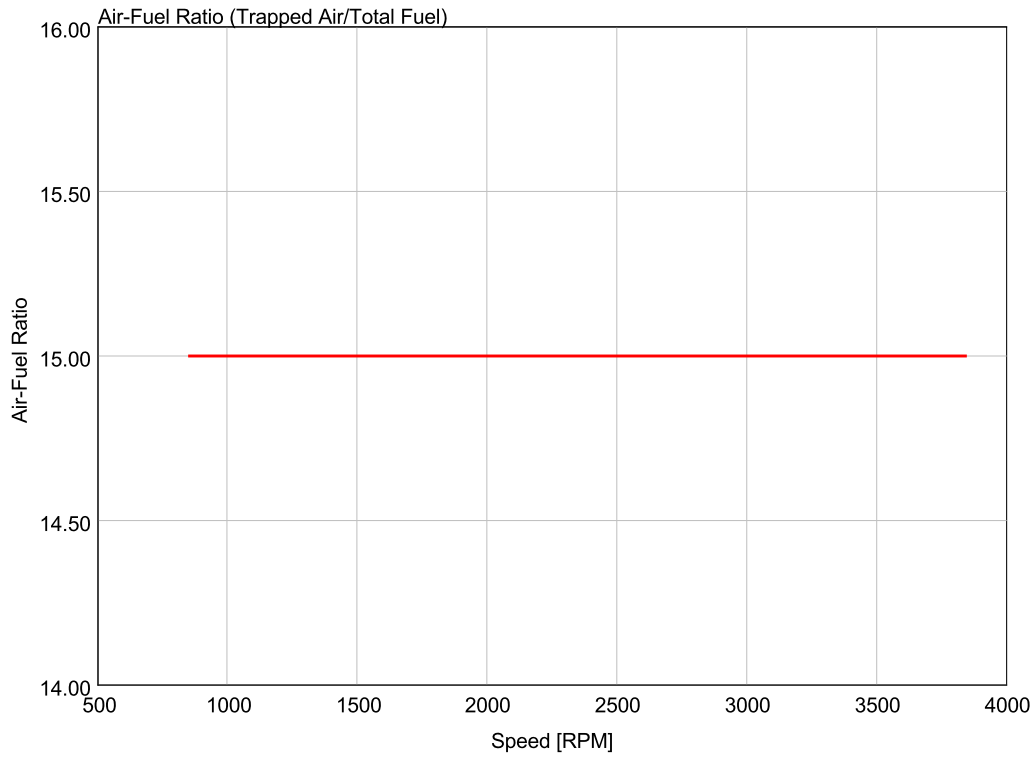


Figure 7.22: Air-to-Fuel ratio

Chapter 8

Conclusions

The objective of the thesis was to develop and validate the methodology that could be used for radial turbine geometrical parameters optimization based on CFD analysis and application to engine performance assessment. The software used in the first part of the simulation, provides good results in different working conditions, even with poorly refined mesh parameters. To create a high quality mesh more calculation power is definitely needed, especially when the geometry gets more complex or if the complete stage of the turbine (including impeller) is considered. In general, the methods developed and the gas implementation have shown good results for this turbine. If no further data are available, the properties of air can be used for diesel exhaust gas calculations. The error associated with neglecting the combustion products is usually no more than about 2%. In a more rigorous approach, corrections must be taken into account for the actual exhaust gas composition (increased H_2O and CO_2 , decreased O_2). An additional difficulty with this approach is the necessity to consider the variable exhaust gas composition, which changes with the engine load factor and the air-to-fuel ratio. Anyways, this specific turbine geometry performs very well under steady-state flow condition, especially for low loads. Losses are limited and the volute manages to develop the fluid by converting the exhaust pressure into kinetic energy to spin the impeller and generate power. Relating to this part, the analysis could be further developed with greater computational power to solve rotating mesh problems, and by performing experimental tests to get practical feedback.

As regards the second part of the thesis, an ad-hoc software was used to carry out the simulations and evaluate the impact of different turbine geometries on the engine performance, using as well data from the 3D model. The standard geometry configuration allows good performance to be obtained for most of the simulated operating points, with slight losses in

terms of efficiency at high regimes. The changes made to the geometry refer to variations in the turbine A/R ratio, by modifying turbine's housing size. Results shown that the reduction of turbine size improves performance (in terms of BSFC) in the region of low loads at the expense of a deterioration that is obtained at higher loads mainly due to the increased backpressure and pumping loss. Respectively, a larger turbine leads to slight improvements in the area of high loads but much more substantial losses in the medium range, explainable considering the higher expansion ratio of the turbine caused by the rack control strategy which is optimized for the standard turbine rather than the modified one.

It should be noted that, turbine's size variations were made using a specific software parameter called "*mass multiplier*", which easily allows to switch from a configuration to another. This was done after making sure that the method won't affect significantly the results of simulation by comparing the scaling method of the software with a reliable method developed after experimental tests.

8.1 Future work

The geometrical design the volute can be further improved by modelling the inlet duct of the volute for a more detailed representation of the turbine.

In terms of CFD simulation, a major step that can be done is the complete study of the turbine including the impeller. That will allow to analyze and study the actual expansion ratio of the turbine and if necessary act on it in order to improve its performance to exploit as much as possible the energy of the exhaust gases. Changing the type of approach to simulation, taking advantage of the data obtained to modify the 3D model of the impeller: the number of blades, the angle and their geometry itself. As previously described, this requires a greater computing power, a greater number of experimental data as well as better knowledge of the entire system. As a further step forward, the study of the entire turbocharger could be performed, by means of simulating both the compressor and the turbine stages together and matching the results to evaluate the real performance of the product and evaluating the response of the compressor.

Regarding GT-Power side, further analysis may be carried out, by means of considering different engine parameters which could be affected by turbocharger variations and their impact on performance.

8.2 Contribution

The thesis work was carried out in close cooperation with the help of dr. inz. Dmytro Samoilenko, in the Erasmus+ Exchange Programme at the Politechnika Warszawska, WUT (Warsaw University of Technology) and completed at the Politecnico di Torino under the supervision of prof. ing. Mirko Baratta. A big thanks goes to them for following and supporting me during this journey.

A special thanks goes to Vittoria, Federico, Marco, Michele and Giovanni for the help and support they gave me during all these years and to Valerio and Giovanni for sustaining me during the last period of my studies.

Finally, my deep and sincere gratitude goes to my father, mother and sister for their continuous help, encouragement, spiritual and economic support. This journey would not have been possible if not for them, and I dedicate this milestone to them.

Bibliography

- [1] H. K. Versteeg, W. Malalasekera, An Introduction to Computational Fluid Dynamics, 2nd Edition, Pearson Education Limited, Edinburgh Gate, Harlow, 2007.
- [2] R. Kabral, M. Abom, Investigation of flow-acoustic interaction in automotive turbocharger, KTH Royal Institute of Technology, Sweden, 2014.
- [3] BorgWarner Turbo Systems, Performance catalogue, Volume 5, 2018.
- [4] Melett, Wabtec Corporation, www.melett.it/technical/types-of-turbocharger.
- [5] Baines, N. C., Fundamentals of Turbocharging Concepts NREC, White River Junction, Vermont, 2005.
- [6] S. Nguyen, Thermodynamics of Turbochargers, Springer, Germany, 2014.
- [7] H. Moustaphe, M. Zelesky, N. Baines, D. Japikse, Axial and Radial Turbines, Concepts NREC, White River Junction, Vermont, 2003.
- [8] SOLIDWORKS, Flow Simulation Technical Reference, Dassault Systemes, 2017.
- [9] GT-Power suite website, www.gtisoft.com/gt-suite-applications/propulsion-systems/gt-power-engine-simulation-software.
- [10] Honeywell Garrett, Original performance, Volume 7, USA, 2015.
- [11] N. Mastorakis, V. Mladenov, Computational Problems in Engineering, Springer, Volume 307 Switzerland, 2014.
- [12] C. Bell, D. Zimmerle, T. Bradley, D. Olsen, P. Young, "Scalable turbocharger performance maps for dynamic state-based engine models", 2016.
- [13] GT-SUITE, Flow Theory Manual, Gamma Technologies, 2014.

- [14] Audi SQ7 TDI V8 TDI with electric powered compressor and 48 volt electrical subsystem, Audi Technology Portal, 3/2016.